HEALTH AND MEDICINE

Pharmacological modulation of mitochondrial calcium uniporter controls lung inflammation in cystic fibrosis

Alessandro Rimessi[1,2]*, Chiara Pozzato[1], Lorenzo Carparelli[1], Alice Rossi[3], Serena Ranucci[3], Ida De Fino[3], Cristina Cigana[3], Anna Talarico[4], Mariusz R. Wieckowski[5], Carla M. P. Ribeiro[6], Claudio Trapella[4], Giacomo Rossi[7], Giulio Cabrini[2,8], Alessandra Bragonzi[3], Paolo Pinton[1,2]*

Mitochondria physically associate with the endoplasmic reticulum to coordinate interorganelle calcium transfer and regulate fundamental cellular processes, including inflammation. Deregulated endoplasmic reticulum–mitochondria cross-talk can occur in cystic fibrosis, contributing to hyperinflammation and disease progression. We demonstrate that *Pseudomonas aeruginosa* infection increases endoplasmic reticulum–mitochondria associations in cystic fibrosis bronchial cells by stabilizing VAPB-PTPIP51 (vesicle-associated membrane protein–associated protein B–protein tyrosine phosphatase interacting protein 51) tethers, affecting autophagy. Impaired autophagy induced mitochondrial unfolding protein response and NLRP3 inflammasome activation, contributing to hyperinflammation. The mechanism by which VAPB-PTPIP51 tethers regulate autophagy in cystic fibrosis involves calcium transfer via mitochondrial calcium uniporter. Mitochondrial calcium uniporter inhibition rectified autophagy and alleviated the inflammatory response in vitro and in vivo, resulting in a valid therapeutic strategy for cystic fibrosis pulmonary disease.

INTRODUCTION

Cystic fibrosis (CF) is a genetic disease caused by mutations of the gene coding for the CF transmembrane conductance regulator (CFTR) protein (*1*). More than 2000 variants and 300 disease-causing mutations have been identified thus far, with the deletion of phenylalanine at position 508 (Phe508del-CFTR) being the most common, affecting approximately 80% of patients with CF in Europe and the United States (*2*). Because of protein misfolding, Phe508del-CFTR is prematurely degraded. In the lungs, the primary organ affected in CF, CFTR gene defects impair chloride transport, reducing water content in the airway surface liquid. This defect increases susceptibility to bacterial infections (such as those by *Pseudomonas aeruginosa*), resulting in hyperinflammation and progressive pulmonary tissue damage, and leading to respiratory insufficiency (*3*). In addition to the lung tissue damage induced by the chronic inflammatory process itself, *P. aeruginosa* has been shown to compromise fundamental processes, including the immune response and the expression of rescued Phe508del-CFTR to the apical membrane (*4*). Thus, the presence of *P. aeruginosa* infection could exacerbate pulmonary CF pathophysiology and render recent CF therapies less effective. Therefore, alternative approaches aimed to activate early anti-inflammatory pathways to prevent organ damage before patients become symptomatic are needed (*5*).

[1]Department of Medical Sciences and Laboratory for Technologies of Advanced Therapies (LTTA), University of Ferrara, 44121 Ferrara, Italy. [2]Center of research on Innovative Therapies for Cystic Fibrosis, University of Ferrara, 44121 Ferrara, Italy. [3]Infections and Cystic Fibrosis Unit, Division of Immunology, Transplantation and Infectious Diseases, IRCCS San Raffaele Scientific Institute, 20132 Milano, Italy. [4]Department of Chemistry and Pharmaceutical Sciences and Laboratory for Technologies of Advanced Therapies (LTTA), University of Ferrara, 44121 Ferrara, Italy. [5]Laboratory of Mitochondrial Biology and Metabolism, Nencki Institute of Experimental Biology, 02-093 Warsaw, Poland. [6]Department of Medicine/Pulmonary Division, Marsico Lung Institute and Cystic Fibrosis Center, Chapel Hill, NC 27599-7248, USA. [7]School of Biosciences and Veterinary Medicine, University of Camerino, 62024 Macerata, Italy. [8]Department of Neurosurgery, Biomedicine and Movement, University of Verona, 37126 Verona, Italy.
*Corresponding author. Email: alessandro.rimessi@unife.it (A.R.); paolo.pinton@unife.it (P.P.)

Mitochondria have recently gained much attention in the medical field due to their involvement in several inflammatory-associated diseases, including CF. Perturbation of mitochondrial activity is sufficient to activate innate immune responses (*6*, *7*), indicating that cells use mitochondrial stress to potentiate innate immunity programs when specific exogenous or endogenous stress alters mitochondrial homeostasis (*8*). The maintenance of functional mitochondria in cells, through mitochondrial stress response and quality control pathways, is thus essential to avoid exacerbation of the inflammatory response. A conserved lysosomal degradation pathway, called mitophagy, controls the quality of mitochondria in stressed cells, acting as a mitochondrial stress response together with the mitochondrial unfolded protein response (UPR^{mt}) (*8*). In relation to CF pathophysiology, a similar mechanism, called xenophagy, plays a role in sequestering and degrading invading pathogens, while macroautophagy controls CFTR intracellular trafficking and function (*9*, *10*). Several protein complexes and signaling pathways, including Ca^{2+} signaling, are involved in these processes (*11*–*13*). However, whether Ca^{2+} signaling and autophagy are directly related to the CF lung–specific pathogenic cascade remains unclear. Impaired Ca^{2+} homeostasis and autophagic defects in CF have been reported, suggesting that both could be directly involved (*7*, *14*–*19*).

We recently demonstrated that the degree and quality of the inflammatory response in CF bronchial cells are supported by *P. aeruginosa*–dependent mitochondrial perturbation, in which the mitochondrial Ca^{2+} uniporter (MCU) is involved in NLRP3 (NOD-, LRR-, and pyrin domain-containing protein 3) inflammasome activation and inflammatory exacerbation in vitro (*7*). Consequently, mitochondrial Ca^{2+} signaling represents a potentially useful but relatively unexploited area for therapeutic innovation and intervention. From this viewpoint, the identified MCU is a strong candidate (*20*). The activity of MCU induces increases in mitochondrial Ca^{2+} concentration with defined timing, amplitude, and kinetics that affect mitochondrial activities, including adenosine triphosphate (ATP) production, inflammation, autophagy, and cell death (*21*, *22*). However, mitochondrial Ca^{2+} homeostasis is primarily conditioned by

the close apposition of mitochondria to endoplasmic reticulum (ER) membranes, which regulates cell fate via inositol 1,4,5-trisphosphate receptors (IP_3Rs) through voltage-dependent anionic channels (VDACs) and MCU (*23*). Miscommunication between the ER and mitochondria occurs in a number of degenerative- and inflammatory-related diseases (*24*); however, whether disrupted ER-mitochondria cross-talk is a consequence of the lung pathological conditions in CF remains elusive. ER-mitochondria contacts, also known as mitochondria-associated ER membranes (MAMs), are multiprotein platforms that appear to tether the two organelles regulating fundamental processes (*24*). The integral ER protein vesicle-associated membrane protein–associated protein B (VAPB) binds the outer mitochondrial membrane protein tyrosine phosphatase interacting protein 51 (PTPIP51) to form some of these tethers (*25*). By manipulating the expression of VAPB or PTPIP51, it is possible to modulate ER-mitochondria contacts, affecting interorganelle Ca^{2+} exchange and autophagy (*26*).

Here, we address the role of the MAM and VAPB-PTPIP51 tether in autophagy during *P. aeruginosa* infection in CF. We show that *P. aeruginosa* infection induces the increase of VAPB and PTPIP51 expression in CF bronchial cells to stabilize ER-mitochondria association, thus affecting autophagy. We demonstrate that defects in CFTR channels lead to reduced selective autophagic clearance capacity during *P. aeruginosa* infection with consequence on mitochondria physiology, inducing persistent UPR^{mt} and NLRP3 inflammasome activation and further down-regulation of the autophagic response and worsening of the inflammatory response in CF bronchial cells. We also show that the mechanism by which VAPB-PTPIP51 tethers regulate autophagy in CF cells involves their key role in mediating interorganelle Ca^{2+} transfer from the ER to mitochondria via MCU. This led us to hypothesize that KB-R7943, an inhibitor of MCU, could be beneficial for alleviating the *P. aeruginosa*–dependent inflammatory response in CF in vitro and in vivo. We show that KB-R7943 is endowed with a unique property, namely, the dual ability to control inflammation and rectify the autophagy response in CF.

RESULTS

The increase of VAPB and PTPIP51 expression impairs autophagy in CF bronchial cells during *P. aeruginosa* infection

To gain insight into the role of ER-mitochondria associations in CF during pathogen infection, we first monitored whether infection with *P. aeruginosa* affected the interaction of key ER-mitochondria Ca^{2+} exchange proteins, such as IP_3R3 and VDAC, using a proximity ligation assay (PLA). Different human non-CF (S9 and NuLi) and CF (IB3-1 and CuFi) bronchial cell models, grown as monolayer on plastic supports, were exposed to *P. aeruginosa* laboratory strain (PAO1) or supernatant from mucopurulent material (SMM) from airways of patients with CF. No changes in IP_3R3-VDAC interactions were quantified in non-CF bronchial cells challenged with *P. aeruginosa* or SMM (Fig. 1A and fig. S1A). In contrast, in CF bronchial cells, challenge with *P. aeruginosa* or SMM increased the interactions between IP_3R3 and VDAC (Fig. 1A and fig. S1A). To test whether the increase in ER-mitochondria contacts was due to altered expression of ER-mitochondria tethers, we probed immunoblots of non-CF and CF bronchial cells exposed for different hours to *P. aeruginosa*. No change in the expression of IP_3R3 and VDAC in both cell lines was detected (fig. S1B), whereas the expression of ER-mitochondria tethers, VAPB and PTPIP51, was increased in CF bronchial cells during pathogen exposure, suggesting that their increase could justify the augmented interaction of IP_3R3 and VDAC (Fig. 1B and fig. S1, C and D). Similar effect on ER-mitochondria tethers has been observed also in polarized mucociliary-differentiated CF patient–derived airway epithelial cells reconstituted on Transwell air-liquid interface (fig. S1E). CF primary airway cells showed enhanced VAPB and PTPIP51 expression compared to wild-type (WT) CFTR-expressing human primary cells when exposed to *P. aeruginosa*, which suggests that defective CFTR channel favors ER-mitochondria interaction during pathogen infection. A major ER-mitochondria interaction in CF bronchial cells when exposed to *P. aeruginosa* or SMM is also confirmed by the enhanced percentage of VAPB-PTPIP51 colocalization (fig. S2A).

By manipulating the expression of VAPB or PTPIP51, it is possible to modulate ER-mitochondria contacts affecting interorganelle Ca^{2+} exchange and autophagy (*26*). We quantified the level of autophagy present in non-CF and CF bronchial cells exposed to *P. aeruginosa* using the most common marker, microtubule-associated protein 1 light chain 3 (LC3) protein. This protein is processed as LC3-I (~16 kDa) and the membrane-bound form LC3-II (~14 kDa), localized to preautophagosomes. By immunoblotting, the level of autophagy was quantified as ratio of LC3-II to LC3-I. *P. aeruginosa* led to significantly down-regulated autophagic response in different CF cellular models compared to non-CF cells under the same experimental conditions, as assessed by a decrease in the LC3-II/LC3-I ratio, which is indicative of defective autophagy (Fig. 1B and fig. S1, D and E). Negative regulation of autophagic machinery in CF cells was also confirmed by microscopy using the green fluorescent protein chimera LC3 (GFP-LC3) to monitor the formation of autophagosomes and by quantifying the number of cells that presented ring-shaped GFP-LC3 structures after pathogen infection. Many cells with ring-shaped GFP-LC3 structures were observed in non-CF cells at different stages of infection (Fig. 1C). A marked reduction in the percentage of GFP-LC3–clustering cells was observed in CF cells, indicating minor processing and translocation of LC3-II from the cytosol to autophagic vacuoles. These data were also confirmed by autophagic flux assay. The levels of LC3-II formation were monitored by immunoblotting in different non-CF and CF bronchial cellular models exposed to *P. aeruginosa* and then treated with saturating concentration of bafilomycin A1. Bafilomycin A1 blocks the fusion of autophagosomes and lysosomes, and by inhibiting LC3-II, degradation may modulate the kinetics of autophagosome synthesis. The ratio of LC3-II/LC3-I in the presence of bafilomycin A1 increased in non-CF cells exposed to *P. aeruginosa*, but this increase was restrained in CF cells, suggesting that the pathogen-induced autophagic flux is reduced in CF cells (Fig. 1D and fig. S2, B and C). The reduction in the autophagic response observed in CF cells, during *P. aeruginosa* infection, could be due to the down-regulation of autophagy as a consequence of the enhanced VAPB-PTPIP51 tethers. To address this issue, we monitored autophagy by manipulating the expression of VAPB and PTPIP51 in non-CF bronchial cells. We transfected S9 cells with empty vector (mock), VAPB, and PTPIP51. This overexpression of VAPB or PTPIP51 markedly increased ER-mitochondria contacts enhancing the interactions between IP_3R3 and VDAC in non-CF cells both under basal conditions and after *P. aeruginosa* exposure (Fig. 1E). Transfection of VAPB or PTPIP51 decreased both the ratio LC3-II/LC3-I (Fig. 1F) and the

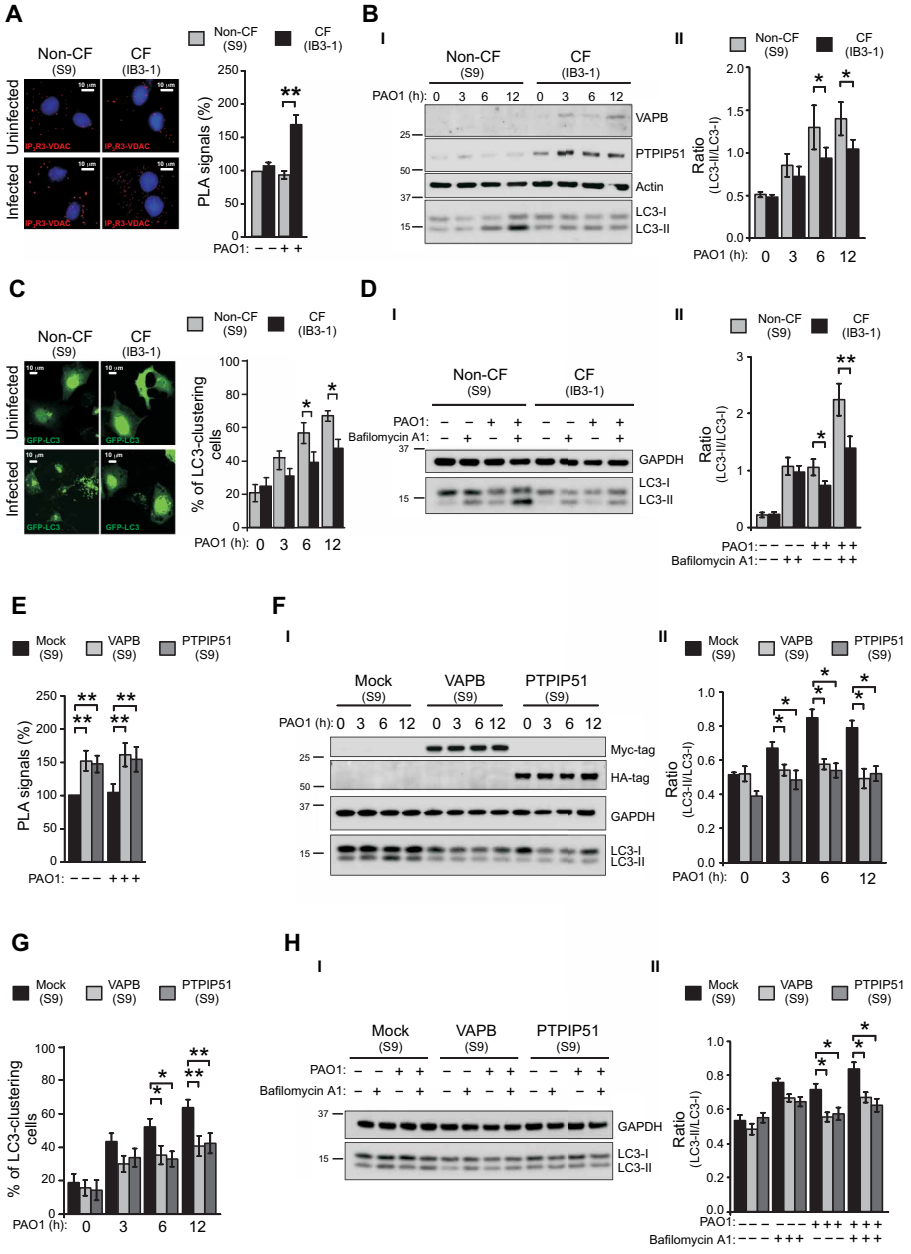

Fig. 1. The increase of ER-mitochondria tethering inhibits autophagy in CF bronchial cells during *P. aeruginosa* infection. (**A**) S9 (non-CF) and IB3-1 cells (CF) were infected with *P. aeruginosa* at an MOI of 100, and after 6 hours, proximity ligation assay (PLA) for IP_3R3 and VDAC interactions was performed. Representative images with PLA signals (red) in the different cells are shown. The cell nuclei were stained with 4′,6-diamidino-2-phenylindole (blue). The bar chart shows quantification of PLA signals (%), respect to uninfected S9 cells ($n = 25$ to 30 independent visual field for each condition of three independent experiments). (**B**) (I) Immunoblots show VAPB and PTPIP51 expression in S9 (non-CF) and IB3-1 (CF) cells during *P. aeruginosa* infection. The cells were uninfected or infected for 3, 6, and 12 hours. The samples were probed using the antibodies indicated, where actin is used as loading control. Protein molecular mass markers are indicated in kilodalton. (II) Bar chart shows the ratio LC3-II/LC3-I following quantification of signals from immunoblots ($n = 5$). (**C**) S9 (non-CF) and IB3-1 cells (CF) were transfected with GFP-LC3–encoding plasmid then infected with *P. aeruginosa*, as indicated. Representative images of GFP-LC3–transfected non-CF and CF cells have been reported. The bars depict the percentage of cells showing the accumulation of GFP-LC3 in cluster ($n = 10$ to 20 independent visual field for each condition of three independent experiments). (**D**) Cells were infected with PAO1 at an MOI of 100 MOI for 6 hours and then treated with either vehicle or bafilomycin A1 (100 nM) as indicated. (I) Samples were probed on immunoblots for LC3 and β-tubulin as a loading control. (II) Bar chart shows the ratio LC3-II/LC3-I following quantification of signals from immunoblots ($n = 10$). (**E**) VAPB or PTPIP51 overexpression increases the IP_3R3-VDAC interactions in S9 cells. The bar chart shows quantification of PLA signals (%) respect to uninfected non-CF mock cells ($n = 45$ independent visual field for each condition of three independent experiments). (**F**) (I) VAPB or PTPIP51 overexpression was probed using Myc-tag and HA-tag antibodies, respectively, while glyceraldehyde-3-phosphate dehydrogenase (GAPDH) is used as a loading control. (II) Bar chart shows the ratio LC3-II/LC3-I following quantification of signals from immunoblots ($n = 4$). (**G**) LC3-clustering cell count in mock and VAPB- or PTPIP51-overexpressing S9 cells during pathogen infection was performed. The bars depict the percentage of cells showing the accumulation of GFP-LC3 in cluster ($n = 40$ independent visual field for each condition of three independent experiments). (**H**) (I) VAPB or PTPIP51 overexpression inhibits autophagic flux in S9 cells during *P. aeruginosa* infection. (II) Bar chart shows the ratio LC3-II/LC3-I following quantification of signals from immunoblots ($n = 6$). The reported data are means ± SE of at least three independent experiments. Student's *t* test was used for indicated comparisons (*$P < 0.05$ and **$P < 0.01$).

percentage of GFP-LC3–clustering cells (Fig. 1G) in non-CF cells exposed to pathogen at different time points. Moreover, whereas treatment with bafilomycin A1 increased the levels of LC3-II in mock non-CF cells, the magnitude of this increase was reduced in VAPB- and PTPIP51-transfected non-CF cells, confirming that the enhanced expression of VAPB or PTPIP51 tethers reduces autophagic response also in non-CF bronchial cells (Fig. 1H).

Effects of *P. aeruginosa*–induced VAPB and PTPIP51 expression on selective autophagic responses

During pathogen infection, selective autophagic responses (mitophagy and xenophagy) contribute together to protect and maintain cellular homeostasis. To test whether their roles could be compromised in CF, we first checked whether *P. aeruginosa* induced a mitophagic response in non-CF and CF bronchial cells. The cells were plated and infected with *P. aeruginosa*, and after intracellular protein fractionation, the expression level and localization of early [optineurin and nuclear dot protein 52 kDa (NDP52)] and late (LC3) mitophagic markers were immunoblotted (Fig. 2A). Optineurin and NDP52 are cytosolic receptors that are also involved in the xenophagic response and are recruited by PINK1 (phosphatase and tensin homolog-induced kinase 1) in the first steps of mitophagy (*27*). They are responsible for recognizing damaged mitochondria migrating to organelles and for promoting their sequestration into autophagosomes. In both cell lines, mitophagic receptors accumulated in the mitochondrial fraction after *P. aeruginosa* infection, triggering the mitophagic response (Fig. 2A and fig. S3A). The reduced mitochondrial redistribution of LC3-II in CF cells suggested slower kinetics of autophagosome synthesis and thus of mitochondrial sequestration compared with non-CF cells (fig. S3A, III). These data were confirmed by colocalization analysis between GFP-LC3 and mitochondrial-targeted red fluorescent protein (mtRFP) (Fig. 2B). As shown by the graph, the number of mitochondria that colocalized with GFP-LC3 clustering was lower in CF cells than in non-CF cells at different stages of pathogen infection. To potentiate the mitophagic response, the kinase PINK1 (phosphatase and tensin homolog–induced kinase 1) phosphorylates Parkin, an E3 ubiquitin ligase that translocates to the altered mitochondria to increase the rate of autophagosome synthesis (*27*).

Using confocal microscopy, we evaluated the levels of Parkin recruited to mitochondria through colocalization analysis between mitochondrial-targeted GFP (mtGFP) and chimeric Parkin cherry. The *P. aeruginosa*–dependent clustering of Parkin to mitochondria in both cell lines was quantified and expressed as the percentage of positive Parkin-clustering cells and as number of mitochondria colocalizing with Parkin clusters for cell (Fig. 2C). In CF bronchial cells, a small percentage of Parkin-clustering cells with respect to non-CF cells was quantified during pathogen infection (Fig. 2, C to I). This reduced amplification of mitophagic response in CF cells was also confirmed by fewer mitochondria colocalization with Parkin cluster (Fig. 2C, II). These results highlight a defect in mitochondrial sequestration during the *P. aeruginosa*–triggered mitophagic response in CF cells, characterized by reduction of the Parkin-mediated amplifying signal.

Although *P. aeruginosa* is primarily considered an extracellular pathogen, reports have demonstrated that, throughout the course of infection, the bacterium acquires the ability to enter and reside within host cells (*28*). CFTR channel defects could also lead to a reduction in xenophagy during pathogen infection, considering that xenophagy and mitophagy are two different events linked by common factors. We measured the xenophagic clearance activity and the *P. aeruginosa* invasion capacity in CF and non-CF bronchial cells. As expected, reduced xenophagic clearance of invading pathogen was detected in CF compared to non-CF cells (Fig. 2D, I). Similar effect on xenophagy has also been confirmed in other CF bronchial cell model and in polarized CF patient–derived airway cells (fig. S3B). In both cases, the higher number of colony-forming unit (CFU) per milliliter of invading bacteria in CF bronchial cells with respect to non-CF indicates a reduction of xenophagic clearance capacity. Through a bacterial invasion assay, we excluded that the accumulation of intracellular bacteria in CF bronchial cells depended on potentiated bacterial invasion (Fig. 2D, II). Last, colocalization analysis was performed between NDP52 and invading pathogens (Fig. 2E). Representative images show the intracellular redistribution of NDP52 around invading bacteria to facilitate sequestration. A reduced percentage of colocalization between NDP52 and invading bacteria was detected in CF bronchial cells with respect to non-CF cells, confirming a minor xenophagic clearance capacity of CF bronchial cells.

These data are in line with the previously described results of mitophagy, confirming that, in CF bronchial cells, defects of CFTR channel led to down-regulation of xenophagic and mitophagic responses with subsequent accumulation of invading bacteria (Fig. 2D and fig. S3B) and dysfunctional mitochondria, characterized by reduced mitochondrial membrane potential ($\Delta\Psi_m$) (fig. S3C) and increased mitochondrial reactive oxygen species (ROS) (fig. S3D).

The defective mitophagy in CF cells could be a crucial mechanism of the *P. aeruginosa*–dependent inflammatory exacerbation because its failure to remove *P. aeruginosa*–damaged mitochondria during infection leads to mitochondrial ROS production and inflammasome activation, with profound effects on cell physiology and cell viability. Similar effects are ascribable to defective xenophagy because impaired degradation of invading bacteria could result in cell stress and pyroptosis induction.

Reduced selective autophagic responses potentiate UPR^{mt} and inflammasome activation, favoring a vicious cycle

Cells sense and respond to mitochondrial dysfunction by activating a protective transcriptional program known as UPR^{mt}, which includes genes that promote mitochondrial protein homeostasis and the recovery of defective organelles. A genetic screen in *Caenorhabditis elegans* identified the transcription factor ATFS-1 (activating transcription factor associated with stress-1) as a key regulator of UPR^{mt}. During mitochondrial dysfunction, ATFS-1 traffics from the cytosol to the nucleus, where it induces transcription of mitochondrial chaperones [HSP10 and HSP60 (heat shock 10 kDa protein and heat shock 60 kDa protein)], proteases [CLPP (Caseinolytic Mitochondrial Matrix Peptidase Proteolytic Subunit)], and antibacterial innate immune genes (*8*). A similar transcriptional response has been described in mammals in which the putative roles of lc ATF4 (activating transcription factor 4) and ATF5, which have considerable homology to ATFS-1, are indicated (*29*). During mitochondrial dysfunction, ATF5 fails to be imported into mitochondria and traffics to the nucleus, inducing gene transcription.

The *P. aeruginosa*–dependent triggering of UPR^{mt} was evaluated by ATF5 and ATF4 nuclear translocation in different CF and non-CF bronchial cellular models. Representative images show the nuclear translocation of both transcription factors in CF cells after

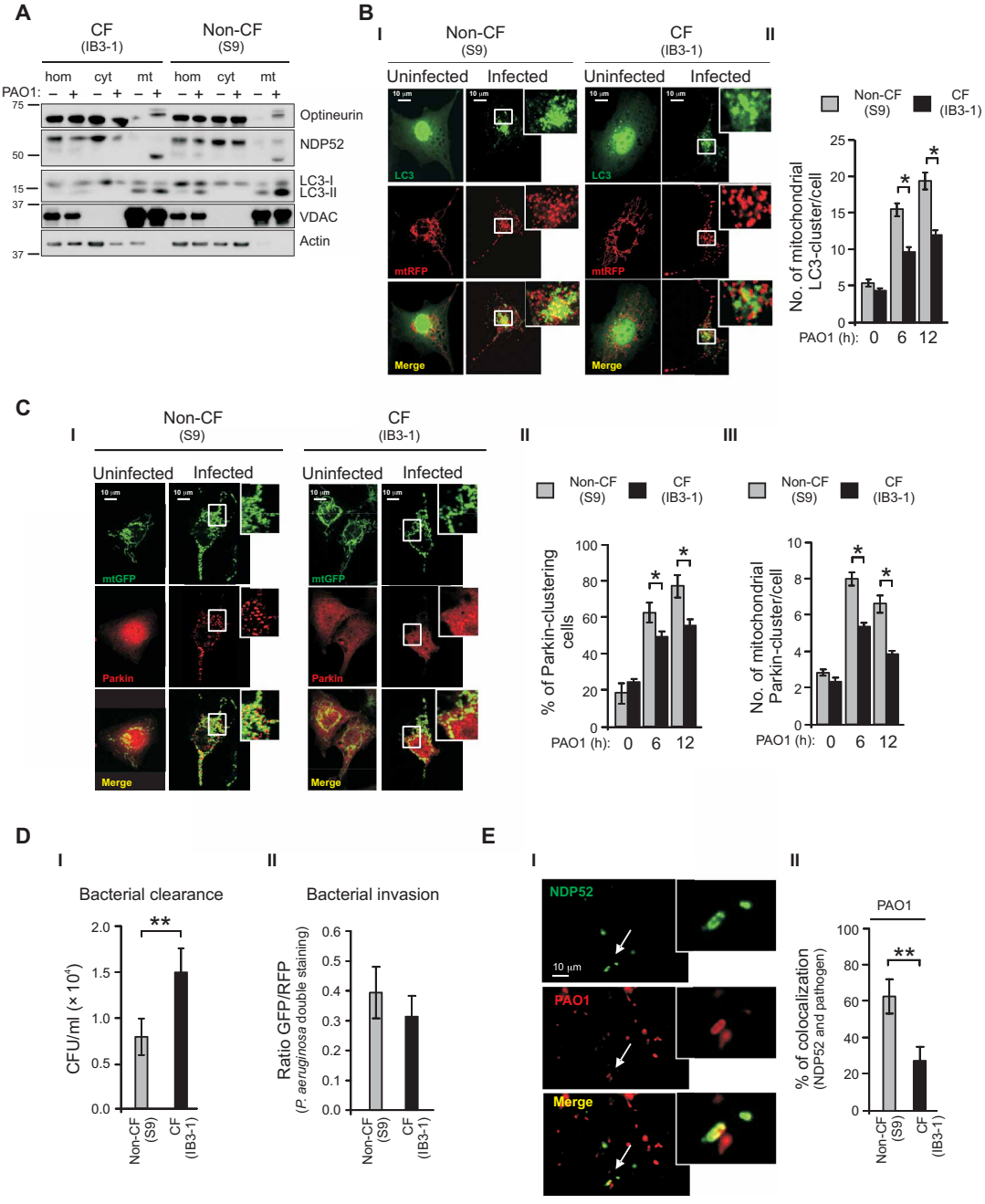

Fig. 2. During *P. aeruginosa* infection the mitophagic and xenophagic response in CF bronchial cells is impaired. (**A**) Uninfected and *P. aeruginosa*–infected airways cells homogenates (hom) of IB3-1 (CF) and S9 (non-CF) cells were fractionated to obtain pure mitochondria (mit) and cytosol (cyt) fractions. Equal amount of proteins (10 μg) from each fraction were analyzed by Western blot using the indicated antibodies. VDAC and actin are, respectively, mitochondrial and cytosolic markers. (**B**) (I) Representative images of S9 and IB3-1 cells cotransfected with GFP-LC3 and mitochondrial RFP and then treated with PAO1 at an MOI of 100 for 6 hours. (II) Quantitative analysis of S9 and IB3-1 cells that contain mitochondria-localized LC3 puncta; the values are expressed as mean number of colocalized-puncta counts per cell (n = 15 to 20 independent visual field for each condition of three independent experiments). (**C**) (I) Representative images of mitochondrial redistribution of Parkin in S9 and IB3-1 cells after *P. aeruginosa* infection. Cells were cotransfected with Parkin cherry and mitochondrial GFP and then treated with PAO1 at an MOI of 100 for 6 hours. (II) The bars depict the percentage of cells showing the accumulation of Parkin in cluster. (III) Quantitative analysis of cells that contain mitochondria-localized Parkin cluster, the values are expressed as mean number of colocalized-cluster counts per cell (n = 20 to 22 independent visual field for each condition of at least three independent experiments). (**D**) (I) Infected S9 and IB3-1 cells were lysed after the addition of impermeable antibiotics and streaked on LB agar plates for the determination of intracellular colony-forming units (CFUs) (n = 8 of independent experiments). (II) Double bacteria labeling and confocal microscopy to quantify bacterial invasion in whole S9 and IB3-1 cells exposed for 6 hours to GFP–*P. aeruginosa*. The bars show the ratio GFP/RFP signal in non-CF and CF bronchial cells, as described in experimental procedure section. (**E**) (I) Representative images of intracellular *P. aeruginosa* internalization and recruitment of NDP52 to pathogen in IB3-1 cells. (II) The bar chart shows quantification of colocalization signals (%) between NDP52 and pathogen in S9 and IB3-1 cells (n = 8 to 13 independent visual field for each condition of at least three independent experiments). The reported data are means ± SE of at least three independent experiments. Paired data were analyzed by Student's t test (*P < 0.05 and **P < 0.01).

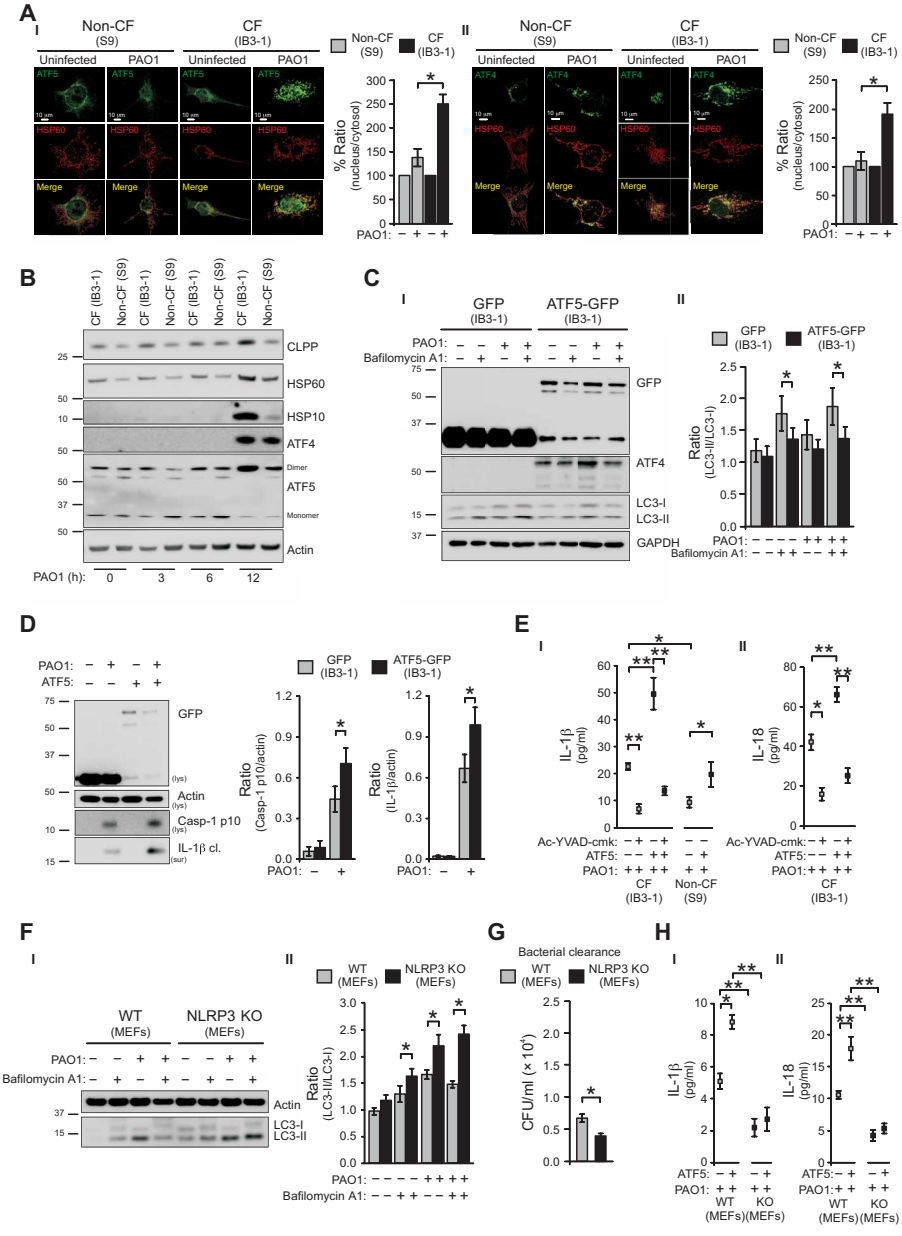

Fig. 3. Abnormal *P. aeruginosa*–dependent UPR^{mt} activation lead to worsening of autophagic defect and of inflammatory response in CF bronchial cells. (**A**) Representative confocal images of nuclear translocation of endogenous ATF5 (I) and ATF4 (II) in S9 (non-CF) and IB3-1 (CF) cells during pathogen infection. The graphs report the nuclear redistribution of ATF5 and ATF4 after PAO1 infection, expressed as percentage increase in fluorescent ratio signals (from cytosol to nucleus) with respect to uninfected condition ($n = 6$ to 10 independent visual field for each condition of three independent experiments). (**B**) Immunoblots of IB3-1 and S9 cells uninfected or infected for 3, 6, and 12 hours, as indicated. The samples were probed using the antibodies indicated, where actin is used as loading control. (**C**) (I) Autophagic flux in IB3-1 cells overexpressing ATF5 during *P. aeruginosa* infection. GFP- and ATF5GFP-transfected cells were infected with PAO1 at 100 MOI for 6 hours and then treated with bafilomycin A1, as indicated. (II) Bar chart shows the ratio LC3-II/LC3-I following quantification of signals from immunoblots ($n = 6$). (**D**) Immunoblots of cleaved caspase-1 and processed IL-1β from lysates (lys) or supernatants (sur) of IB3-1 and ATF5-overexpressed IB3-1 cells infected for 6 hours with *P. aeruginosa*. Actin was used as loading control. The quantification is expressed as the ratio of casp-1–p10/actin and cleaved IL-1β/actin. The bars are the means ± SE of four independent immunoblots. (**E**) IB3-1 and S9 cells were transfected with ATF5-GFP and after 6 hours of PAO1 infection, and the cultured cell supernatant were collected to quantify the levels of proinflammatory cytokines by enzyme-linked immunosorbent assay (ELISA) ($n = 5$ of independent experiments). The selective inhibitor of caspase-1, 20 μM Ac-YVAD-cmk, was added 30 min before infection. (**F**) Murine WT and NLRP3-null (NLRP3 KO)–derived embryonic fibroblasts (MEFs) were infected with PAO1 at an MOI of 100 for 6 hours and then treated with either vehicle or bafilomycin A1 as indicated. (I) Samples were probed on immunoblots for LC3 and actin as a loading control. (II) Bar chart shows the ratio LC3-II/LC3-I following quantification of signals from immunoblots ($n = 4$). The reported data are means ± SE of at least three independent experiments. (**G**) Infected WT and NLRP3 KO MEFs were lysed after the addition of impermeable antibiotics and streaked on LB agar plates for the determination of intracellular CFUs ($n = 3$ of independent experiments). (**H**) WT and NLRP3 KO MEFs were transfected with ATF5-GFP and after 6 hours of PAO1 infection, and the cultured cell supernatant were collected to quantify the levels of proinflammatory cytokines by ELISA ($n = 3$ of independent experiments). Paired data were analyzed by Student's *t* test (*$P < 0.05$ and **$P < 0.01$).

P. aeruginosa infection (Fig. 3A and fig. S4A). Major ATF5 and ATF4 nuclear redistribution was measured in CF cells with respect to non-CF cells challenged with *P. aeruginosa*, suggesting that UPR^{mt} is mainly induced in CF cells (Fig. 3A and fig. S4A). *P. aeruginosa*–dependent UPR^{mt} activation was also monitored by immunoblotting and quantification of UPR^{mt} reporters, such as HSP10, HSP60, and CLPP (Fig. 3B and fig. S4, B and C). Increased expression levels of UPR^{mt} reporters followed the abnormal UPR^{mt} induction promoted by the stabilization of ATF5 and ATF4 in CF cells during pathogen infection. Similar results were also obtained in polarized CF patient–derived airway cells, where the stabilization and dimerization of ATF5, induced by *P. aeruginosa* infection, corresponded to an increment of UPR^{mt} reporters (fig. S4D).

Considering the defective mitophagy and consequent accumulation of dysfunctional mitochondria, persistent activation of UPR^{mt} was assessed in CF cells when exposed to pathogen infection. Since ATF5 has been shown to suppress autophagy in human BCR-ABL–transformed cells (*30*), we questioned whether the stabilization of ATF5 in CF cells, and thus the persistent UPR^{mt} activation, affected *P. aeruginosa*–triggered autophagy and inflammation. To mimic UPR^{mt} hyperactivation, we transfected the chimera ATF5-GFP into CF bronchial cells. This overexpression favored the stabilization of ATF4 and markedly increased the susceptibility to *P. aeruginosa*–triggered UPR^{mt} activation, enhancing the expression level of UPR^{mt} reporters in CF cells, both under basal conditions and upon *P. aeruginosa* infection (Fig. 3C and fig. S5A). Moreover, transfection of different CF bronchial cellular models with ATF5, then exposed to *P. aeruginosa*, decreased the LC3-II/LC3-I ratio according to the autophagic flux assay, indicating that persistent UPR^{mt} activation in CF cells during pathogen infection further decreases the rate of autophagic response (Fig. 3C and fig. S5B). ATF5 overexpression resulted in enhanced inflammatory sensitivity to pathogen infection in CF bronchial cells, as shown by increased expression level of cleaved caspase-1 and cleaved cytokine interleukin–1β (IL-1β) in cell supernatant (Fig. 3D and fig. S5C) and by higher level of inflammasome-dependent IL-1β and IL-18 release (Fig. 3E and fig. S5D). The forced expression of ATF5 strengthened the inflammasome-dependent IL-1β release after incubation with *P. aeruginosa* in non-CF bronchial cells (Fig. 3, E to I, and fig. S5, D to I), the same cells, where the presence of wt CFTR mitigates the *P. aeruginosa*–dependent mitochondrial effects, avoiding NLRP3 inflammasome activation (*7*).

However, the exacerbation of the *P. aeruginosa*–triggered inflammation promoted by ATF5 overexpression was attenuated by the pretreatment with caspase-1 inhibitor Ac-YVAD-cmk (20 μM), which, by affecting the inflammasome, reduced the release of cytokines (Fig. 3E and fig. S5D) and ameliorated the rate of autophagic response in CF bronchial cells (fig. S5E). These results confirm that the synergy between *P. aeruginosa*–dependent mitochondrial stress and consequent abnormal UPR^{mt} activation leads to worsening of autophagic defects and inflammatory responses in CF cells.

Additional data obtained in NLRP3 knockout (KO) and WT mouse embryonic fibroblasts (MEFs) suggested that the down-regulation of autophagy during *P. aeruginosa* infection is also strictly related to NLRP3 inflammasome activation (Fig. 3F). By autophagic flux assay, the LC3-II conversion in the presence of bafilomycin A1 increased in WT fibroblasts, but this increase was augmented in NLRP3 KO fibroblasts, both under basal condition and after *P. aeruginosa* infection, indicating that loss of NLRP3 stimulates autophagic flux. NLRP3 deficiency augmented bacterial clearance capacity in NLRP3 KO MEFs with respect to WT MEFs (Fig. 3G), while the NLRP3 activator nigericin (10 μM) treatment reduced the bacterial clearance capacity in CF bronchial cells, enhancing further the number of CFU per milliliter of invading pathogen (fig. S5F). Last, the deletion of NLRP3 in MEFs prevented the inflammasome-dependent IL-1β and IL-18 release in ATF5-overexpressing NLRP3 KO MEFs during *P. aeruginosa* infection (Fig. 3H). Collectively, these findings show that the worsening of defective autophagy in CF bronchial cells, started by *P. aeruginosa*–induced VAPB and PTPIP51 expression, is also sustained by abnormal UPR^{mt} and NLRP3 inflammasome activation, contributing to persistent accumulation of damaged mitochondria and invading bacteria.

Regulation of ER-mitochondria tethering controls Ca^{2+} exchange and abrogates the effects of tethering on autophagy

The expression of VABP or PTPIP51 both led to an increase in IP_3R3-VDAC interactions (fig. S6A). We monitored whether overexpression of VAPB or PTPIP51 affected the uptake of Ca^{2+} by mitochondria following IP_3R-mediated release from the ER store. For these experiments, we cotransfected, in different CF bronchial cellular models, empty vector (pcDNA3), VAPB, or PTPIP51 and mitochondrial-targeted aequorin Ca^{2+} probe. We triggered physiological IP_3R-mediated Ca^{2+} release by stimulation with 100 μM histamine. As expected, transfection of both VAPB and PTPIP51 induced a significant increase in mitochondrial Ca^{2+} response (Fig. 4A and fig. S6B) and had no effects on cytosolic Ca^{2+} levels (fig. S6C). We therefore investigated whether the reduction in autophagy induced by VAPB or PTPIP51 overexpression is caused by a higher Ca^{2+} transfer to mitochondrial matrix. To verify this hypothesis, we first quantified the changes in IP_3R3-VDAC interactions by PLA in MCU-silenced CF bronchial cells (shMCU-CF cells) transfected with pcDNA3, VAPB, or PTPIP51 during pathogen infection or SMM treatment (Fig. 4B and fig. S6D). The silencing of MCU induced a reduction in the protein expression (fig. S6E) and in histamine-dependent mitochondrial Ca^{2+} uptake (fig. S6F) without affecting the $\Delta\Psi_m$ (fig. S6G). The reduction in mitochondrial Ca^{2+} uptake in shMCU-CF cells protected the mitochondria from *P. aeruginosa*–dependent $\Delta\Psi_m$ loss, decreasing mitochondrial superoxide production and NLRP3 activation (*7*). The maintenance of mitochondrial physiology in shMCU-CF cells during *P. aeruginosa* infection is also confirmed by lacked *P. aeruginosa*–triggering nuclear translocation of transcription factors ATF5 and ATF4, avoiding the UPR^{mt} activation (fig. S6H).

Under basal conditions, the overexpression of VAPB or PTPIP51 increased the association between the two ER-mitochondria Ca^{2+} exchange proteins, IP_3R3-VDAC in shMCU-CF cells. In contrast, no significant differences emerged between empty vector–transfected shMCU-CF cells (pcDNA3) and nonsilenced CF cells (Mock). In CF cells, *P. aeruginosa* exposure led to a marked enhancement of IP_3R3-VDAC PLA signaling (Figs. 1A and 4B). This increase was abrogated both in pcDNA3-transfected shMCU-CF cells and in VAPB- or PTPIP51-overexpressing shMCU-CF cells, indicating that the changes in IP_3R3-VDAC interactions during pathogen infection are strictly dependent on MCU (Fig. 4B). The gain of IP_3R3-VDAC interaction in CF bronchial cells exposed to *P. aeruginosa* or SMM could be the consequence of compensatory responses that promote the increase of VAPB and PTPIP51 expression, at front of pathogen-dependent mitochondrial perturbations, which impairs $\Delta\Psi_m$ and thus Ca^{2+} uptake into the mitochondrial matrix.

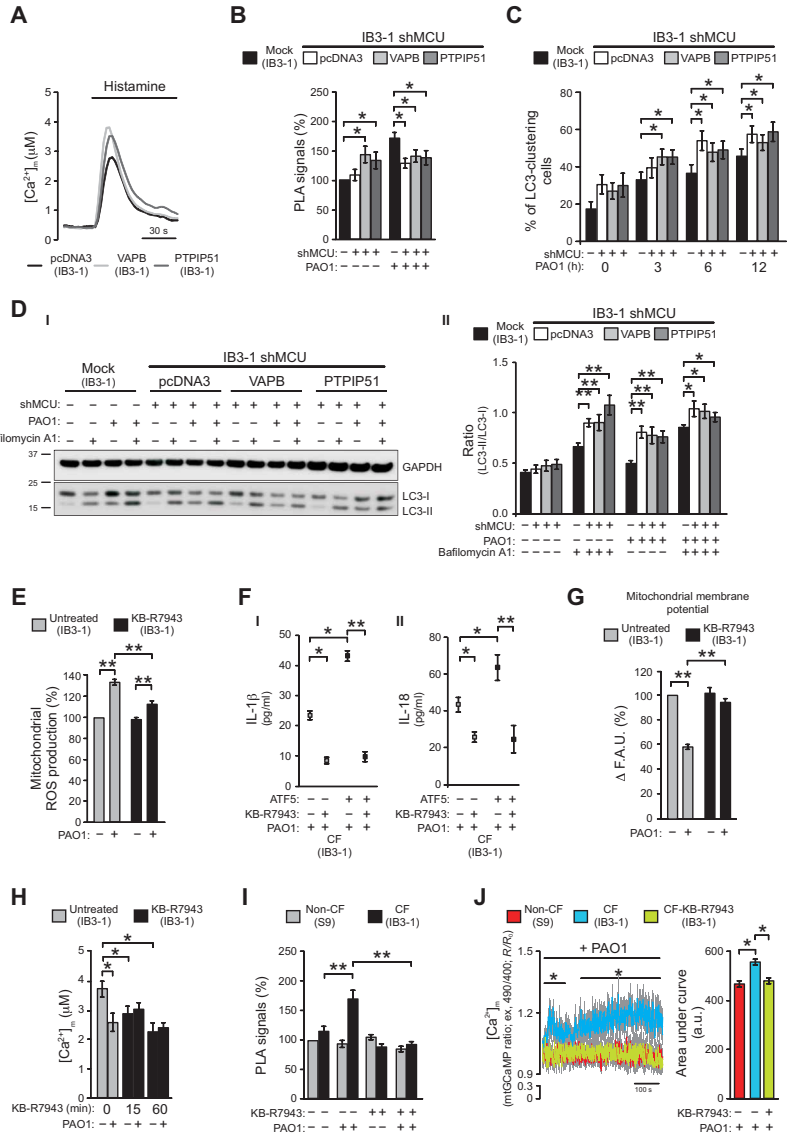

Fig. 4. MCU targeting abrogates the effects of VAPB and PTPIP51 on autophagy, restoring the mitochondrial physiology in CF bronchial cells exposed to pathogen. (**A**) Mitochondrial Ca^{2+} response in IB3-1 cells (CF cells) overexpressing VAPB or PTPIP51; representative traces are shown. Cells were cotransfected with mitochondrial-targeted aequorin with control empty vector (pcDNA3), VAPB, or PTPIP51 and stimulated with 100 μM histamine. (**B**) Stable MCU-silenced IB3-1 clone (IB3-1 shMCU) was transfected with pcDNA3, VAPB, or PTPIP51 and then infected with PAO1 at an MOI of 100 for 6 hours. PLA for IP_3R3 and VDAC interactions was performed. The bar chart shows quantification of PLA signals (%), with respect to uninfected IB3-1 cells (mock) ($n = 15$ independent visual field for each condition of three independent experiments). (**C**) LC3-clusteing cell count in pcDNA3 and VAPB- or PTPIP51-overexpressing IB3-1 shMCU cells during pathogen infection was performed. The bars depict the percentage of cells showing the accumulation of GFP-LC3 in cluster ($n = 25$ independent visual field for each condition of at least three independent experiments). (**D**) Effects of VAPB and PTPIP51 on autophagic flux in IB3-1 shMCU cells during pathogen infection. (I) Samples were probed on immunoblots for LC3 and GAPDH as a loading control. (II) Bar chart shows the ratio LC3-II/LC3-I following quantification of signals from immunoblots ($n = 6$). (**E**) The effects of MCU-inhibition by 1 μM KB-R7943 pretreatment on superoxide production in CF bronchial cells during PAO1 infection. The quantification of percentage change of cells positive for MitoSox staining compared with uninfected IB3-1 cells is shown ($n = 8$ independent experiments). (**F**) Levels of IL-1β and IL-18 in KB-R7943–treated mock and ATF5-overexpressing IB3-1 cells, collected after 6 hours of PAO1 infection at an MOI of 100 ($n = 10$ independent experiments). (**G**) Measurements of mitochondrial ΔΨ in KB-R7943–treated and untreated IB3-1 cells during bacterial infection. The bars show the change in the TMRM fluorescence level before and after treatment with *P. aeruginosa* strain, expressed as the percentage change with respect to untreated IB3-1 cells. FCCP was used to collapse the mitochondrial ΔΨ ($n = 12$ independent experiments). F.A.U., fluorescent arbitrary units. (**H**) Histamine-dependent mitochondrial Ca^{2+} responses of KB-R7943 pretreating IB3-1 cells at different time points before and after PAO1 infection. The histograms show all means ± SE of mitochondrial Ca^{2+} responses ($n = 5$ independent experiments). (**I**) S9 (non-CF) and IB3-1 cells (CF) were pretreated with KB-R7943 1 hour before the infection with PAO1 at an MOI of 100. PLA for IP_3R3 and VDAC interactions was performed. The bar chart shows quantification of PLA signals (%), with respect to uninfected S9 cells ($n = 15$ independent visual field for each condition). The reported data are as means ± SE of at least three independent experiments. (**J**) Mitochondrial Ca^{2+} dynamics in S9- (non-CF), IB3-1– (CF), and KB-R7943–treated IB3-1 (CF-KB-R7943) cells exposed to PAO1 at an MOI of 100 were evaluated through ratiometric imaging of mitochondrial-targeted GCaMP6. Traces represent means ± SE of mitochondrial Ca^{2+} response from at least of 10 independent experiments. SE values are illustrated using gray shading. For statistical significance, the multiple Student's *t* test has been used. The bar chart shows the quantification of the area under the curve. a.u., arbitrary unit. Student's *t* test used for indicated comparisons (*$P < 0.05$ and **$P < 0.01$).

We also monitored how MCU silencing affected autophagy in VAPB- or PTPIP51-overexpressing CF cells. MCU silencing in CF cells, challenged with *P. aeruginosa*, induced a significant increase in the percentage of GFP-LC3–clustering cells with respect to naive CF cells (Fig. 4C). However, the inhibitory effects of VAPB and PTPIP51 overexpression on the percentage of GFP-LC3–clustering cells were abrogated in shMCU-CF cells exposed to *P. aeruginosa* (Fig. 4C). Moreover, treatment with bafilomycin A1 not only confirmed that the silencing of MCU increased the LC3-II/LC3-I ratio, demonstrating an induction of autophagy, but also showed that this increase was unaffected by overexpression of VAPB or PTPIP51 (Fig. 4D). Thus, the inhibitory effect of VAPB and PTPIP51 on autophagy in CF bronchial cells is lost by blocking mitochondrial Ca^{2+} uptake. In this case, it is also possible to prevent the increase in IP_3R3-VDAC interactions during pathogen infection due to *P. aeruginosa*–induced VAPB and PTPIP51 expression (Fig. 4B).

MCU inhibition limits the *P. aeruginosa*–dependent inflammatory response and mitochondrial stress, promoting autophagy

All these results identify MCU as a candidate target to limit *P. aeruginosa*–mediated hyperinflammation in the CF lung, raising the question of its druggability in the CF inflammatory model. In this view, we tested the MCU inhibitor KB-R7943 (1 μM), pretreating CF bronchial cells 1 hour before challenging with *P. aeruginosa*. The selected concentration of drug is useful to partially reduce mitochondrial Ca^{2+} uptake in CF bronchial cells. KB-R7943, which was developed to inhibit the reverse mode of Na^+/Ca^{2+} exchange (NCX) in intact cells, a lower concentration has been shown to be a potent MCU inhibitor, an effect that contributes to its protective activity (*31*). In addition, given that CF cells (IB3-1) used in our in vitro experiments lack any plasma membrane (PM) NCX activity (*32*), KB-R7943 could be considered a specific MCU inhibitor in these CF cells. KB-R7943 pretreatment prevented *P. aeruginosa*–triggered mitochondrial dysfunction in CF bronchial cells, reducing mitochondrial ROS production (Fig. 4E), inflammasome activation (fig. S7A), and the inflammasome-dependent IL-1β and IL-18 release (Fig. 4F and fig. S7B). The anti-inflammatory effect of KB-R7943 was also confirmed by reduced levels of IL-1β and IL-18 released in the culture supernatants of ATF5-overexpressing CF cells after exposition to bacteria, abrogating the amplification of *P. aeruginosa*–triggered inflammasome response induced by abnormal UPR^{mt} activation (Fig. 4F and fig. S7B).

Reports have purported that the protective effect of KB-R7943 is due in part to mild $\Delta\Psi_m$ depolarization and/or complex I inhibition (*33*, *34*). Successively, these considerations have been questioned, demonstrating that KB-R7943 has no negative impact on mitochondrial respiration and $\Delta\Psi_m$ (*35*). However, KB-R7943 pretreatment did not alter $\Delta\Psi_m$ in CF bronchial cells under basal condition, excluding an effect on the mitochondrial respiratory capacity and $\Delta\Psi_m$ (Fig. 4G); KB-R7943 prevented $\Delta\Psi_m$ loss observed in CF bronchial cells upon prolonged pathogen infection (Fig. 4G). The effect of MCU inhibition on intracellular Ca^{2+} signaling was evaluated using aequorin-based measurement. KB-R7943 alone induced a reduction in histamine-dependent mitochondrial Ca^{2+} response in CF cells (Fig. 4H and fig. S7C) without affecting cytosolic transient and ER Ca^{2+} content (fig. S7D), indicating once more that the effect of KB-R7943 on mitochondrial Ca^{2+} signaling is not ascribable to perturbed mitochondrial respiratory capacity but only to the selective inhibition of MCU. No differences in histamine-dependent mitochondrial (Fig. 4H) and cytosolic (fig. S7E) Ca^{2+} responses were emerged between *P. aeruginosa*–infected KB-R7943–treated CF cells and uninfected KB-R7943–treated CF cells. The lacked synergistic reduction of mitochondrial Ca^{2+} response in *P. aeruginosa*–infected KB-R7943–treated CF cells (in theory, due to KB-R7943–dependent MCU inhibition and to *P. aeruginosa*–induced $\Delta\Psi_m$ dissipation) demonstrates that KB-R7943 through the inhibition of MCU preserves the $\Delta\Psi_m$ during pathogen infection, preventing mitochondrial damage that could further affect the mitochondrial Ca^{2+} uptake capacity of CF bronchial cells (Fig. 4H).

We also demonstrated that, when preventing *P. aeruginosa*–dependent mitochondrial dysfunction by KB-R7943, the increases in IP_3R3-VDAC interactions during bacterial infection or SMM were lost (Fig. 4I). We suppose that the exacerbation of the *P. aeruginosa*–triggered inflammatory response is mitigated by MCU inhibition, which avoids a mitochondrial Ca^{2+} overload due to compensatory increased ER-mitochondria interaction, which, in turn, favors a higher ER-mitochondria Ca^{2+} transfer in CF bronchial cells during pathogen infection. To demonstrate this, we performed mitochondrial Ca^{2+} measurement using the ultrasensitive mitochondrial GFP-based Ca^{2+} probe, mtGCaMP6, useful to measure fast and small mitochondrial Ca^{2+} change (Fig. 4J and fig. S7F). Acute exposure of CF bronchial cells to *P. aeruginosa* or SMM induced a sustained increase of mitochondrial Ca^{2+} concentration (Fig. 4J and fig. S7F). Conversely, by inhibiting MCU with KB-R7943, the mitochondrial Ca^{2+} uptake in CF bronchial cells exposed to pathogen or SMM was abrogated. No perturbation in mitochondrial Ca^{2+} signaling was detected in non-CF bronchial cells when exposed to *P. aeruginosa* or SMM (Fig. 4J and fig. S7F), confirming a higher ER-mitochondria Ca^{2+} transfer in CF bronchial cells. The concept of mitochondrial Ca^{2+} overload, however, does not necessarily refer solely to a very large increase in mitochondrial Ca^{2+} concentration, rather much smaller, but prolonged, increases of Ca^{2+} may activate the organelle dysfunctional machinery, leading to $\Delta\Psi_m$ dissipation, reduced ATP production, increased release of ROS, protein tyrosine phosphatase opening, and mitochondria swelling (*20*).

Then, we monitored whether KB-R7943 affected autophagy in CF bronchial cells when exposed to *P. aeruginosa*. The higher LC3-II/LC3-I ratio (Fig. 5A and fig. S8A) and percentage of GFP-LC3–clustering cells (Fig. 5B) in KB-R7943–treated CF cells than in untreated CF cells indicated recovery of autophagy during infection. Treatment with bafilomycin A1 confirmed that KB-R7943 pretreatment, by preventing mitochondrial Ca^{2+} overload, increased the LC3-II/LC3-I ratio in CF cells upon *P. aeruginosa* challenge and thus autophagy (Fig. 5C). However, the increase in LC3-II/LC3-I ratio (Fig. 5D) and percentage of GFP-LC3–clustering cells (Fig. 5E) in KB-R7943–treated CF cells exposed to the pathogen were unaffected by overexpression of tethers, VAPB or PTPIP51. The recovery of autophagy in KB-R7943–treated CF cells, by MCU inhibition, potentiated the bacterial clearance activity in different CF bronchial cell models when exposed to bacteria (Fig. 5F and fig. S8B), ameliorating cell viability (Fig. 5G and fig. S8C). To exclude the possibility that KB-R7943 has toxic effects on bacterial viability and proliferation, we evaluated *P. aeruginosa* growth under different concentrations of KB-R7943. No changes in the bacterial growth curve emerged (fig. S8D). In line with the data of MCU silencing, the inhibition of mitochondrial Ca^{2+} uptake abrogates the inhibitory effects of VAPB and PTPIP51 on autophagy in CF bronchial cells, promoting cell resistance to pathogen infection.

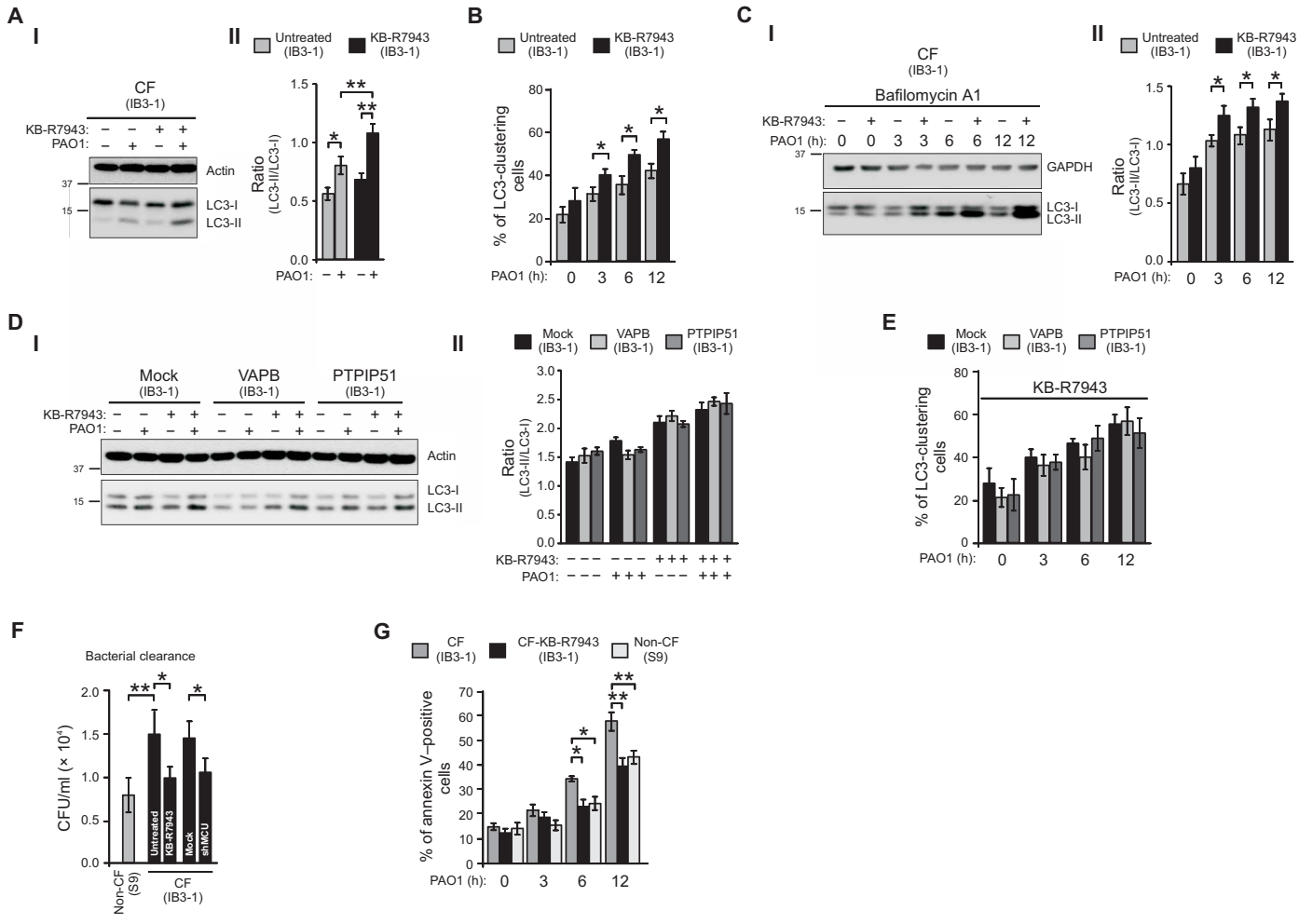

Fig. 5. KB-R7943 restores the autophagic response in CF bronchial cells. (**A**) (I) Immunoblot of untreated and KB-R7943–treated IB3-1 cells infected with PAO1 at an MOI of 100 for 6 hours. The samples were probed for LC3 and actin as a loading control. (II) Bar chart shows the ratio LC3-II/LC3-I following quantification of signals from immunoblots ($n = 5$). (**B**) LC3-clustering cell count in untreated and KB-R7943–treating IB3-1 cells was performed. The bars depict the percentage of cells showing the accumulation of GFP-LC3 in cluster during *P. aeruginosa* infection ($n = 20$ independent visual field for each condition of at least three independent experiments). (**C**) Effects of KB-R7943 on autophagic flux in IB3-1 cells during pathogen infection. (I) Samples were probed on immunoblot for LC3 and GAPDH as a loading control. (II) Bar chart shows the ratio LC3-II/LC3-I following quantification of signals from immunoblots ($n = 6$). (**D**) Immunoblots of mock and VAPB- and PTPIP51-overexpressing IB3-1 cells pretreated with KB-R7943 1 hour before *P. aeruginosa* infection, as indicated. (I) Samples were probed on immunoblot for LC3 and actin as a loading control. (II) Bar chart shows the ratio LC3-II/LC3-I following quantification of signals from immunoblots ($n = 6$). (**E**) LC3-clustering cell count was performed in mock and VAPB- or PTPIP51-overexpressing IB3-1 cells exposed to MCU-inhibitor, KB-R7943, and PAO1 at an MOI of 100, as indicated. The bars show the percentage of cells showing the accumulation of GFP-LC3 in cluster ($n = 20$ independent visual field for each condition of at least three independent experiments). (**F**) S9, KB-R7943–treating IB3-1 cells, and/or IB3-1 shMCU cells were infected with PAO1 at an MOI of 100 for 6 hours and then lysed after the addition of impermeable antibiotics and streaked on LB agar plates for the determination of intracellular CFUs ($n = 10$ of independent experiments). (**G**) Effect of KB-R7943 on IB3-1 cell apoptosis, during *P. aeruginosa* infection, using annexin V Alexa Fluor 488/propidium iodide staining. Cells were plated in 60-mm plates and treated for 1 hour with KB-R7943 before PAO1 infection, as indicated. Cell viability and death were evaluated using a Tali apoptosis kit and the Tali image-based cytometer. Bars show the percentage of IB3-1 (CF) and S9 (non-CF) cells that were annexin V–fluorescein isothiocyanate–positive ($n = 6$ independent experiments). The reported data are means ± SE of at least three independent experiments. Student's *t* test was used for indicated comparisons (*$P < 0.05$ and **$P < 0.01$).

KB-R7943 mitigates the *P. aeruginosa*–triggered inflammatory response in vivo

Last, we analyzed the efficacy of KB-R7943 in counteracting pathogenic CF lung inflammation in vivo. C57Bl/6 Cftr^{tm1UNC}TgN(FABPCFTR)#Jaw (CFTR-KO) mice and their WT (non-CF) littermates were infected with *P. aeruginosa* AA43 clinical isolate embedded in agar beads and treated with KB-R7943 (300 μg/kg) or vehicle (ctrl) via aerosol administration by the Penn-Century MicroSprayer Aerosolizer. The schedule of treatment was 1 hour before infection and then every 12 hours. Two days after infection and 1 hour after the last treatment, murine lungs and bronchialalveolar lavage fluid (BALF) were collected and processed. First, we evaluated the KB-R7943 distribution in tissues of treated mice by mass spectrometry. The drug was detected both in the lung homogenates [677.1 ± 305.6 pg/ml (WT) versus

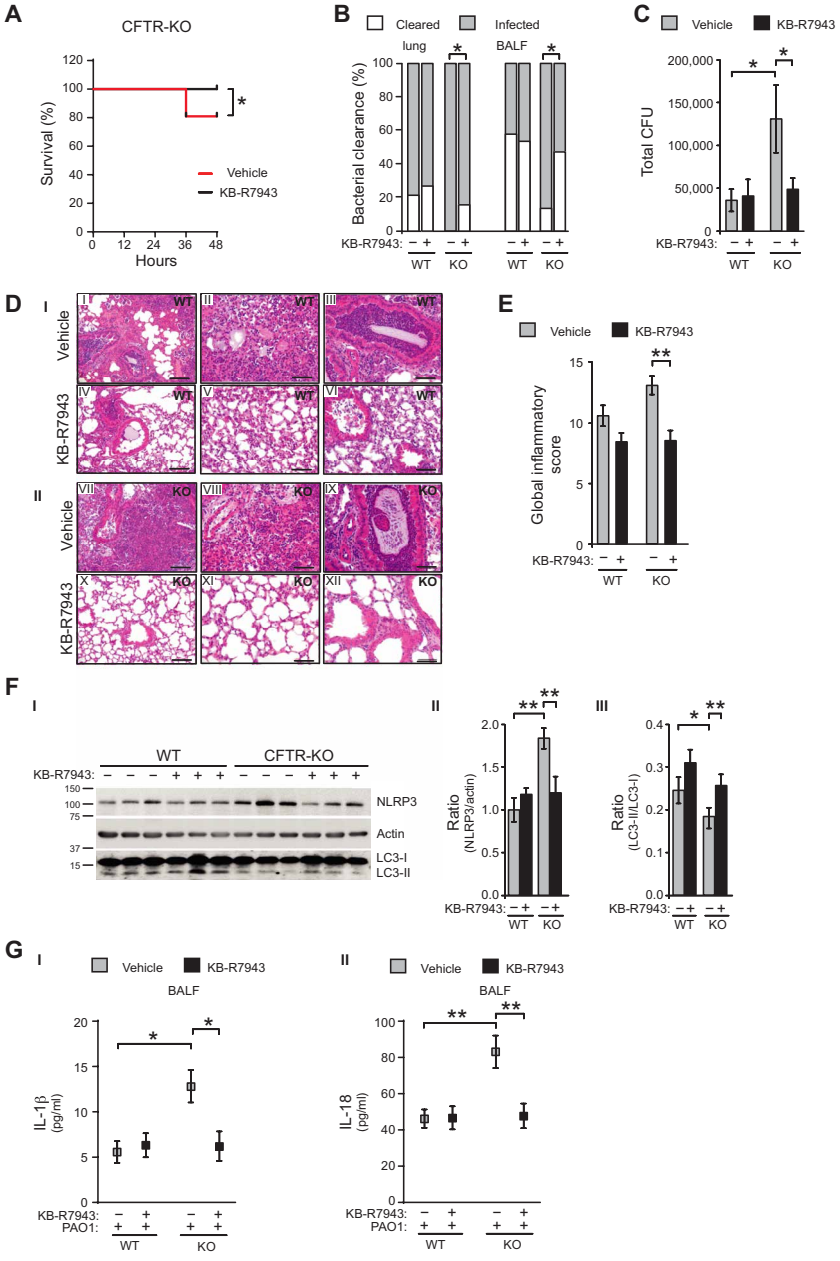

Fig. 6. KB-R7943 limits the *P. aeruginosa*–triggered inflammatory response in CF mice. C57BL/6 ^{Cftrtm1}UNCTgN(FABPCFTR)#Jaw mice (CFTR-KO) ($n = 20$ for each experimental condition) and their WT littermates ($n = 20$ for each experimental condition) were inoculated with 1.5×10^6 CFU of *P. aeruginosa* AA43 isolate embedded in agar beads. Mice were treated with KB-R7943 (300 μg/kg) or vehicle via aerosol administration by the Penn-Century MicroSprayer Aerosolizer every 12 hours starting 1 hour before infection. Every 12 hours, mice were monitored for the health status. Two days after infection, 1 hour after the last treatment, murine lungs and BALFs were collected and processed. (**A**) Kaplan-Meier survival curve for untreated and KB-R7943–treated CFTR-KO mice. The data were analyzed by log-rank (Mantel-Cox) test and Gehan-Breslow-Wilcoxon test ($P = 0.0378$; GraphPad Prism, USA) ($n = 20$ mice for each condition of three independent experiments). (**B**) Clearance and infection were determined on surviving mice. The data were analyzed by Fisher's test (confidence intervals, 95%; $^*P < 0.05$; GraphPad Prism, USA) ($n = 20$ mice for each condition of three independent experiments). (**C**) Bacterial burden in the lungs of KB-R7943–treated and untreated mice after 2 days from *P. aeruginosa* challenge is shown. Bar chart represent means ± SE of lung CFU in mice. Data were analyzed by two-way ANOVA and Tukey's post hoc test ($^*P < 0.05$, $n = 15$ mice analyzed of three independent experiments). (**D**) The images exemplify the lungs of WT and CFTR-KO mice stained with hematoxylin and eosin (H&E), pretreated 1 hour before infection with KB-R7943 and vehicle. Scale bars, 250 μm (I, IV, VII, and X) and 500 μm (II, III, V, VI, VIII, IX, XI, and XII). (**E**) Graphs summarize histological scoring of global inflammation grading based on H&E staining ($n = 15$ of independent experiments). Data were analyzed by Student's *t* test used for indicated comparisons and by two-way ANOVA and Tukey's post hoc test ($^{**}P < 0.01$). (**F**) (I) Immunoblots show NLRP3 and LC3 expression in murine WT and CFTR-KO lung homogenates after *P. aeruginosa* infection. The samples were probed on immunoblots for NLRP3, LC3, and actin as a loading control. Bar chart shows the ratio NLRP3/actin (II) and ratio LC3-II/LC3-I (III) following quantification of signals from immunoblots (n =9 to 12). Student's *t* test was used for indicated comparisons ($^*P < 0.05$ and $^{**}P < 0.01$). (**G**) The levels of released IL-1β (I) and IL-18 (II) were measured in BALF of WT and CFTR-KO mice exposed to *P. aeruginosa* infection, treated with KB-R7943 (300 μg/kg) and vehicle. The data were analyzed by two-way ANOVA and Tukey's post hoc test ($^*P < 0.05$ and $^{**}P < 0.01$; $n = 25$ of independent experiments).

703.3 ± 150.3 pg/ml (CFTR-KO)] and in plasma [194.3 ± 87.3 pg/ml (WT) versus 173.9 ± 56.8 pg/ml (CFTR-KO)], confirming that it is a permeable and stable drug (fig. S9A).

To define the therapeutic effect of KB-R7943 in CFTR-KO and WT mice, we measured the survival, bacterial burden, and inflammatory response. Survival of CFTR-KO mice after *P. aeruginosa* infection was significantly improved by KB-R7943 treatment [80% (vehicle) versus 100% (KB-R7943)] (Fig. 6A). In addition, KB-R7943 treatment of CFTR-KO mice led to significantly increased clearance of *P. aeruginosa* infection both in the lung and BALF (Fig. 6B), with significant decrease of bacterial burden (Fig. 6C and fig. S9B) compared to vehicle. Differently, both KB-R7943 and vehicle-treated WT mice survived to infection and did not show differences in bacterial clearance (Fig. 6B) or bacterial burden (Fig. 6C and fig. S9B). These results show that KB-R7943 impacts on a better health status and *P. aeruginosa* infection in CFTR-KO mice.

Lung histopathology and the degree of inflammation were investigated by scoring global inflammatory response, extension, and type in tissue sections of murine lungs stained with hematoxylin and eosin (H&E) (Fig. 6, D and E, and fig. S8, C and D). In CFTR-KO and, in part, in WT mice, *P. aeruginosa* infection favored the diffusion of a massive exudate in lungs (Fig. 6D, I and VII), with a large involvement of alveolar spaces and broncho-bronchiolar lumina that markedly reduced the aerate areas (Fig. 6D, II, III, VIII, and IX). KB-R7943 treatment reduced the inflammatory status in CFTR-KO lungs. A marked reduction of the inflammatory cells in alveoli and deep airways was documented (Fig. 6D, IV, V, VI, X, XI, and XII) in KB-R7943–treated mice compared to vehicle. Moreover, *P. aeruginosa* infection significantly increased histological inflammation scores, which were diminished when the animals were pretreated with KB-R7943 (Fig. 6E and fig. S9, C and D).

In vivo, the pretreatment with KB-R7943 in CFTR-KO mice reduced NLRP3 inflammasome expression in the lung homogenates after infection to levels detected in ctrl WT mice, thus preventing the *P. aeruginosa*–triggered NLRP3 inflammasome priming observed in vehicle-treated CFTR-KO mice (Fig. 6F). In line with the data in vitro, the higher LC3-II/LC3-I ratio in KB-R7943–treated CFTR-KO mice than in vehicle-treated CFTR-KO mice confirmed the recovery of autophagy in vivo (Fig. 6F).

Last, the efficacy of KB-R7943 on the exacerbated *P. aeruginosa*–triggered inflammation in CF was confirmed by the reduced IL-1β and IL-18 levels detected in BALF of treated CFTR-KO mice (Fig. 6G). Conversely, no significant differences in inflammatory cells and tumor necrosis factor–α (TNFα) levels between KB-R7943 and vehicle-treated mice were detected (fig. S9, E and F), suggesting that the "first proinflammatory signal," or Toll-like receptor signaling, in both lungs is unchanged with the drug treatment. The reduction of released cytokines in BALF is due to rectified autophagy and escaped *P. aeruginosa*–dependent mitochondrial dysfunction, avoiding thus abnormal UPR^{mt} and NLRP3 inflammasome activation in KB-R7943–treated CFTR-KO mice.

DISCUSSION

The excessive inflammatory response due to chronic airway infection by *P. aeruginosa* plays a critical role in the CF lung pathology and disease progression. Within the innovative CF therapy pipeline, including CFTR "correctors" and "potentiators," effective and alternative anti-inflammatory drugs are lacking. CFTR correctors and potentiators have garnered much attention in the CF community, although their impact on downstream consequences, such as inflammation, has been debated. Evidence shows that *P. aeruginosa* burden decreased in the first 6 months of modulator therapy but rebounded thereafter, increasing the inflammatory response (*36*).

A number of bacterial pathogens perturb mitochondrial function to promote proliferation and infection, such as *P. aeruginosa*. Conversely, mitochondria present different roles in resistance against bacterial infection, including mitochondrial ROS production and inflammasome activation (*37*, *38*), and protective roles, such as mitophagy and UPR_{mt} (*8*, *39*).

Previous data showed that CFTR-defective bronchial cells have increased intracellular [Ca^{2+}] associated to increased susceptibility to pathogen-dependent mitochondrial dysfunction (*7*). The perturbed Ca^{2+} homeostasis in patients with CF underlies the compromising mechanisms of mitochondrial stress response and quality control pathways. The prolonged and abnormal UPR^{mt} activation is the negative consequence of the down-regulation of selective autophagic response in CF, which leads to an increase in pathogen survival, resulting in enhanced innate immune and mitochondrial-protective gene expression (*40*) and, ultimately, worsen pulmonary inflammation (Fig. 3).

During infection, the interactions between ER and mitochondria change to sustain a range of physiological processes. This structural perturbation is proposed to represent a physiological response of the cell to altered mitochondrial bioenergetics during infection because mitochondria require Ca^{2+} for efficient production of ATP (*41*). ER-mitochondria interactions arise as a result of ER-resident VAPB closely associated with mitochondrial protein PTPIP51, enabling ER membrane recruitment to mitochondria. Here, we reported that *P. aeruginosa*–induced VAPB-PTPIP51 tether regulates autophagy in CF bronchial cells. The increase of VAPB and PTPIP51 expression triggered by bacterial infection in CF bronchial cells induces tightening of the tether and concomitant impairment of autophagy (Figs. 1 and 2). We also demonstrated that blocking the ER-mitochondria Ca^{2+} exchange via MCU-targeted short hairpin RNA (shRNA) or pharmacological inhibition, by KB-R7943, abrogates the effects of VAPB and PTPIP51 on autophagy in CF cells during bacterial infection (Figs. 4 and 5). Our findings are in line with a large number of studies that show that perturbation of Ca^{2+} delivery to mitochondria stimulates autophagy and mitophagy (*11*, *42*, *43*).

Our discoveries about the regulation of mitophagy and UPR^{mt} in CF during *P. aeruginosa* infection have suggested a therapeutic strategy to promote the overall health of the mitochondrial network to limit the CF lung disease progression and bacterial infection. Consistent with the ability of KB-R7943 to reduce CF pulmonary inflammation, the promotion of autophagy appeared to contribute to the protective activity of KB-R7943.

Our findings qualify KB-R7943 as a mitochondrial Ca^{2+} regulator that rectifies unbalanced autophagic activity controlling UPR^{mt} and NLRP3 inflammasome activation, known to contribute significantly to pathologic airway inflammation in CF (*7*). The cross-regulation between autophagy and inflammasomes may also explain the ability of KB-R7943 to limit *P. aeruginosa*–triggered NLRP3 inflammasome priming in the lungs of CFTR-KO mice in vivo (Fig. 6) (*44*, *45*).

According to our study, mitochondrial Ca^{2+} regulators have emerged as a new option for CF therapy in controlling inflammation and bacterial infection. Currently, there are two specific MCU inhibitors, ruthenium red and Ru360, which are known to be

impermeable to the PM (*20*). In 2017, a high-throughput assay that screened for human MCU-specific small-molecule modulators identified mitoxantrone as selective inhibitor of MCU among more than 600 clinically approved drugs. Unfortunately, mitoxantrone was toxic after 48 hours of treatment, independent of its action on MCU (*46*). Despite mechanistic limitations and the availability of newer, more selective MCU inhibitors, KB-R7943 is the first available MCU inhibitor, which is freely permeable through the PM, with protective activity (*31*). KB-R7943, which was developed to inhibit the reverse mode of NCX in intact cells (*47*), has been shown to protect against myocardial ischemia-reperfusion injury and neuronal damage (*34*, *48*, *49*). The effect of KB-R7943 is about threefold more selective for NCX3 than for NCX1 and NCX2 (*50*), and NCX3 is the only isoform that is also located on the outer mitochondrial membrane involved in the regulation of mitochondrial Ca^{2+} homeostasis (*51*).

The mechanism through which KB-R7943 confers protection remains controversial and debated. If used at concentrations up to 1 μM, KB-R7943 may inhibit a variety of ion channels (Na^+, K^+, and Ca^{2+}), neurotransmitters receptors (nicotinic and *N*-methyl-D-aspartate), and store-operated Ca^{2+} entry (*52*). In the kidney, KB-R7943 increases renal vascular resistance, causing vasoconstriction that may be harmful (*53*), and is toxic to cancer cells at high concentrations (30 μM and more) by inducing apoptosis and affecting autophagy (*54*). The nonspecificity of the molecule and its toxicity at high concentrations have long limited the clinical usefulness of KB-R7943. Nevertheless, it remains an important pharmacological tool in the laboratory setting to define and develop new therapeutic approaches.

Here, we show that KB-R7943 is endowed with unique activity to correct CF pulmonary physiopathology through the regulation of autophagy and inflammation. Although KB-R7943 appears to play roles in multiple activities through which it may rectify *P. aeruginosa*–triggered autophagy and preserve mitochondrial homeostasis, inhibition of mitochondrial Ca^{2+} signaling appears to be a key to these mechanisms, as well as considering that the CF bronchial cells used for in vitro experiments lack any PM NCX activity (*32*).

Through its multitasking activity, KB-R7943 treatment could represent viable strategy to rectify the multifunctional defect in individuals with CF. Airway epithelia absorb Na^+ through the epithelial Na^+ channel (ENaC), which is negatively regulated by CFTR. In patients with CF, the absence of CFTR results in an ENaC hyperactivity and increased Na^+ absorption (*55*). This increase results in membrane depolarization that activates the NCX reverse mode, promoting a further influx of Ca^{2+} in CF cells (*56*). Intracellular Ca^{2+} overload provides a positive feedback loop for autophagy and chloride secretion inhibition and mitochondrial dysfunction (*13*, *57*–*60*). This indicates that KB-R7943 could be exploited in CF for pharmacologic correction of outcomes related to (i) intracellular Ca^{2+} overload through inhibition of PM NCX reverse mode and (ii) mitochondrial Ca^{2+} overload through the simultaneous inhibition of MCU and NCX3 reverse mode. In this view, KB-R7943 represents an excellent example of a multitasking drug with anti-inflammatory effects that can also favor rescuing of chloride secretion and CFTR functioning in patient with CF, ameliorating airways disease.

METHODS

Antibodies and other reagents

For immunoblot and immunostaining, the following antibodies were used:

anti-actin (A3853), anti-LC3 (L7543), and anti–β-tubulin (T5201; all from Sigma-Aldrich); anti-MCU (ab121499), anti-myc (ab9106), anti-ATF5 (ab60126), anti-pseudomonas (ab68538), anti-VAPB (ab196487), anti-PTPIP51 (ab224081), and anti-VDAC (ab15895; all from Abcam); anti-GFP (sc9996), anti–hemagglutinin (HA) (sc7392), anti-HSP60 (sc13115), anti-mitofusin 2 (MFN2) (sc50331), and anti-HSP10 (sc20958; all from Santa Cruz Biotechnology); anti-CLPP (14181), anti-ATF4 (11815), anti–glyceraldehyde-3-phosphate dehydrogenase (2118), anti–IL-1β (12242), and anti-NDP52 (9036; all from Cell Signaling Technology); anti-optineurin (10837-1-AP, ProteinTech); anti–caspase-1 (NB100-56565, Novus Biologicals); anti-NLRP3 (ag20boo14, AdipoGen); and anti-IP_3R3 (BD Biosciences). All the reagents were from Sigma-Aldrich, unless otherwise indicated. KB-R7943 (sc202681) was dissolved in dimethyl sulfoxide and was from Santa Cruz Biotechnology.

Cell culture, transfection, and infection

IB3-1 cells (CF cells) are human bronchial epithelial cells derived from patient with CF with a mutant ΔF508/W1282X genotype. The CF phenotype of the IB3-1 cells was corrected in the S9 cell line (non-CF cells; non-CF) by transfection with WT adeno-associated virus expressing CFTR. Both cells were grown on plastic support under liquid-liquid conditions in LHC-8 basal medium (Life Technologies) supplemented with 5% fetal bovine serum.

CuFi-1 (CF cells) and NuLi cells (non-CF) were a gift from J. Zabner (University of Iowa). The CuFi-1 cells were derived from human bronchial epithelia from a patient with CF (CFTR mutant genotype ΔF508/ΔF508), and the NuLi cells were derived from the normal lung of a 36-year-old patient. These cells were grown under liquid-liquid conditions on human placental collagen-coated flasks (Sigma-Aldrich) with bronchial epithelial growth medium (Lonza).

The CF patient–derived cells are represented by polarized mucociliary-differentiated human airway epithelium that was reconstituted in vitro using cells isolated from patient (MucilAir Epithelix CF-202; a 24-year-old female with homozygous $\Delta F_{508}/F_{508}$) and grown on Transwell air-liquid interface. The wt CFTR human primary cells are represented by polarized mucociliary-differentiated human airway epithelium that was reconstituted in vitro with cells isolated from donor (MucilAir Epithelix; MD-801, a 59-year-old female donor with no pathology reported) and grown on Transwell air-liquid interface.

Stable MCU-silencing IB3-1 cell clone was obtained using shRNA targeting MCU (TRCN0000133861) purchased from Sigma-Aldrich. IB3-1 cells were cultured in tissue dish to 75% of confluence and infected with lentiviral-driven shRNA targeting MCU for 48 hours. The infected cells were selected by the addition of 5 μM puromycin to the culture medium, fed every 2 to 3 days with selection medium, and checked for cell death after 3 to 7 days. Resistant cells were normally observed after about 2 weeks of selection. Individual cells were selected randomly and placed in separate wells within a 24-well plate. Clones were grown to confluency and expanded in a maintenance puromycin media (0.5 μM). Expanded clones were retested for MCU expression before any further studies. Primary $Nlrp3^{+/+}$ and $Nlrp3^{-/-}$ MEFs were cultured in Dulbecco's Modified Eagle Medium supplemented with 10% fetal bovine serum (Life Technologies) and 1% penicillin-streptomycin-glutamine (100×) liquid.

For the transient overexpression experiments, pNEO plasmid encoding a myc-tagged VAPB and a HA-tagged PTPIP51 and ATF5

cloned in pEGFP-N1 were transfected with Lipofectamine LTX (Life Technologies) according to the manufacturer's recommendations. After 36 hours, the transfected cells were infected with the well-characterized, motile, nonmucoid *P. aeruginosa* laboratory strains, named PAO1, donated by A. Prince (Columbia University). Bacterial colonies from overnight cultures on trypticase soy agar (Difco) plates were grown in 20 ml of trypticase soy broth (Difco) at 37°C with shaking until an optical density (OD_{660nm}) corresponding to 1×10^7 CFU/ml was reached. The bacteria were washed twice with Krebs-Ringer buffer (KRB), and diluted in each specific serum-free medium before infection. PAO1 was added to cells as indicated in the captions for Figs. 1 through 5.

Mucopurulent material was harvested from the lumens of excised human CF lungs infected with *P. aeruginosa* at the UNC Adult Cystic Fibrosis Center. SMM from several patients was pooled to assure homogeneous stimulus throughout the experiments. Ten microliters of SMM (1:100) or KRB (a control for SMM) was applied to cells for 6 hours.

Proximity ligation assay

PLAs to quantify IP_3R3-VDAC interactions were performed in according to the manufacturer's protocol of Duolink reagents (Sigma-Aldrich). Cells were fixed in 4% paraformaldehyde in KRB and probed with mouse IP_3R3 (BD Biosciences) and rabbit anti-VDAC1 (Abcam) antibodies. Signals were developed using a Duolink In Situ Far Red kit. Images were acquired with digital imaging system based on a Zeiss Axiovert 200 fluorescence microscope (20× objective) and quantified using ImageJ.

Immunoblotting

Briefly, to obtain whole-cell extracts, cells were washed, harvested, and lysed in radioimmunoprecipitation assay buffer supplemented with 2 mM Na_3VO_4, 2 mM NaF, 1 mM phenylmethylsulfonyl fluoride, and complete protease inhibitor cocktail (Roche Diagnostics Corp.).

Thereafter, protein extracts were separated on precast 4 to 12% SDS–polyacrylamide gel electrophoresis gels (Life Technologies), electrotransferred onto polyvinylidene difluoride membranes (Bio-Rad), and probed with the specific antibodies. Last, the membranes were incubated with the appropriate horseradish peroxidase–conjugated secondary antibodies (SouthernBiotech), followed by chemiluminescence detection using West Pico reagent (Thermo Scientific Pierce). The immunoreactive bands were acquired using the ImageQuant LAS-4000 system (GE Healthcare) and quantified using ImageJ. The immunoblots shown are representative of at least three independent experiments.

Immunofluorescence

After infection, the cells were washed with KBR and fixed in 4% paraformaldehyde for 10 min. Then, cells were permeabilized for 10 min with 0.1% Triton X-100 in KBR and blocked in KBR containing 2% bovine serum albumin and 0.05% Triton X-100 for 1 hour. Cells were then incubated with primary antibody overnight at 4°C and washed three times with KBR. The appropriate isotype-matched, Alexa Fluor–conjugated secondary antibodies (Life Technologies) were used. Images were taken with a Nikon Swept Field confocal equipped with CFI Plan Apo VC60XH objective [numerical aperture (NA), 1.4] (Nikon Instruments) and an Andor DU885 electron multiplying charge-coupled device camera (Andor Technology Ltd.).

Ca^{2+} measurements

For cytosolic aequorin and mitochondrial aequorin measurements, cells growing on coverslips were incubated with 5 μM coelenterazine for 2 hours in KRB supplemented with 1% fetal calf serum and then transferred to the perfusion chamber. To reconstitute the aequorin chimeras targeted to the ER, the luminal $[Ca^{2+}]$ of this compartment had to be first reduced by incubating the cells for 1 hour at 4°C in KRB supplemented with 5 μM ionomycin and 600 μM EGTA in the presence of 5 μM coelenterazine, followed by extensive washing of the cells with KRB supplemented with 2% BSA and 1 mM EGTA. All aequorin measurements were performed in KRB supplemented with 1 mM $CaCl_2$, and agonists and other drugs were added to the same medium, as specified in the figure legends. Experiments terminated by lysing the cells with 100 μM digitonin in a hypotonic, Ca^{2+}-rich solution to discharge the remaining aequorin pool. The output of the discriminator was captured by a Thorn EMI photon counting board and stored in an IBM-compatible computer for further analyses. The aequorin luminescence data were calibrated offline into $[Ca^{2+}]$ values using a computer algorithm based on the Ca^{2+} response curve of WT and mutant aequorins.

Microscopy analysis

For autophagic and mitophagic count, the cells were seeded and then transfected with LC3 in pEGFP-C1 and Parkin cherry, respectively. After 36 hours, images were taken on a Zeiss Axiovert 200 fluorescence microscope (63×, 40×, or 20× objectives). For each condition, the number of GFP-LC3 or Parkin cherry–clustering cells was counted in at least 10 to 20 independent visual fields and expressed as percentage. For colocalization analysis, the cells were seeded and then cotransfected with mtRFP and GFP-LC3 or mtGFP and Parkin cherry using Lipofectamine LTX. After 36 hours, coverslips were placed in an incubated chamber with controlled temperature, CO_2, and humidity, and z stacks at 21 planes and a distance of 0.2 μm were taken to allow acquisition of the entire cell. The images were restored with the AutoQuant three-dimensional blind deconvolution module and loaded into Imaris 4.0 (Bitplane AG). Obtained puncta images were merged to compare the GFP signals with RFP or cherry signals using ImageJ software. For each condition, the colocalization of these two signals was quantified in at least 20 independent visual fields, expressing the data as number of LC3 or Parkin dots localized to mitochondria/cell.

Subcellular fractionation

After infection, the cells (10^9) were harvested, washed two times with KBR, resuspended in homogenization buffer [225 mM mannitol, 75 mM sucrose, 30 mM tris-HCl (pH 7.4), 0.1 mM EGTA, and phenylmethylsulfonyl fluoride], and gently disrupted by Dounce homogenization. The homogenate was centrifuged twice at 600*g* for 5 min to remove nuclei and unbroken cells. The supernatant was then centrifuged at 10,300*g* for 10 min to pellet crude mitochondria. The crude mitochondrial fraction was resuspended in isolation buffer [250 mM mannitol, 5 mM Hepes (pH 7.4), and 0.5 mM EGTA] and then subjected to Percoll gradient centrifugation [Percoll medium: 225 mM mannitol, 25 mM Hepes (pH 7.4), 1 mM EGTA, and 30% (v/v) Percoll]. After centrifugation at 95,000*g* for 30 min (SW40 rotor), a dense band containing purified mitochondria was collected, washed by centrifugation at 6300*g* for 10 min to remove the Percoll, and lastly, resuspended in isolation medium.

Bacterial clearance

Bacterial killing was performed infecting human airway epithelial cell with GFP-expressing *P. aeruginosa* strains (ampicillin resistant strains) at different multiplicities of infection (MOIs). Briefly, the cells were infected in serum-free LHC-8 media with ampicillin-resistant *P. aeruginosa* strain at an MOI of 1:10 and 1:100 for 6 hours. Extracellular bacteria were killed with cell-impermeable antibiotics [penicillin-streptomycin (50 U/ml each; Life Technologies) and gentamycin (200 μg/ml; Life Technologies)]. Cells were then washed in KBR and lysed in KBR containing 0.2% Triton X-100 (Sigma-Aldrich), and a serial dilution of lysate was streaked in duplicate on ampicillin-selected LB (lysogeny broth) agar plates and incubated overnight at 37°C. The day after, CFUs were counted. Samples containing no cells were used to identify background CFUs, which were subtracted from samples.

Bacterial invasion

Double bacteria labeling, confocal microscopy, and image analysis allow identification and quantification of the number of internalized bacteria. To identify intracellular and extracellular bacteria, images from whole cells were analyzed in three steps. First, a binary mask of the *P. aeruginosa* antibody channel (594 nm) highlighting extracellular bacteria was generated. Then, the mask was subtracted from the bacterial channel (GFP-expressing *P. aeruginosa* strains; 488 nm), giving intracellular bacteria as a result. Last, the logical AND operation was performed between the mask and the bacterial channel, giving extracellular bacteria as a result. Images of pathological and non-CF cells infected with GFP-expressing *P. aeruginosa* and stained with anti–*P. aeruginosa* antibody were acquired. All data are expressed as ratio between the 488- and 594-nm signal.

ROS production measurements

Mitochondrial ROS production was measured by staining cells in KBR for 15 min at room temperature with 5 μM MitoSox Red (Life Technologies) and successively analyzed on a Tali image-based cytometer (Life Technologies).

Mitochondrial membrane potential measurements

Cells were loaded with 10 nM tetramethylrhodamine methyl ester (TMRM) (Life Technologies) at 37°C for 20 min, placed in a humidified chamber, and imaged with a LiveScan Swept Field Confocal Microscope (Nikon Instruments Inc.) equipped with a 60× oil immersion lens. To completely collapse, the electrical gradient established by respiratory chain FCCP (carbonyl cyanide *p*-trifluoromethoxyphenylhydrazone; 10 μM) was added. All data are expressed as percentage of the total TMRM fluorescence minus the TMRM fluorescence after FCCP treatment.

Mitochondrial targeted GCaMP6m measurements

To test $[Ca^{2+}]_m$ with high sensitivity, a Ca^{2+} probe based on the last-generation GCaMP probe was generated, targeted to the mitochondrial matrix. We chose the GCaMP6m version due to its highest Ca^{2+} affinity (K_d of 167 nM). To be truly quantitative, we took advantage of the isosbestic point in the GCaMP6m excitation spectrum, in living cells exciting GCaMP6m at 400 nm leads to fluorescence emission, which is not Ca^{2+} dependent.

S9 and IB3-1 cells were grown on 24-mm coverslips and transfected with mtGCaMP6m-encoding plasmid. After 36 hours, coverslips were placed in one ml of modified KRB (5.5 mM glucose and 1 mM $CaCl_2$), and imaging was performed on an Olympus Xcellence widefield system equipped with a 40×/1.3 NA Oil Plan Fluor objective. Excitation was performed at 490 and 400 nm, and one field was collected per coverslip. Images were captured each 500 ms, and after the first 50 frames, PAO-1 (MOI of 100) or SMM (MOI of 1:100) was added to cells as indicated in the figure. Analysis was performed with ImageJ where both images were background and corrected frame by frame. The data are presented as the means ± SE of the ratio of all time points of all the experiments, using Prism (GraphPad Prism, USA), and we have calculated the area under curve for each experiments.

Cell viability assay

Cells were plated in 60-mm plates and pretreated with 1 μM KB-R7943 for 1 hour before PAO1 infection. Cells were harvested 72 hours after treatment and stained using annexin V Alexa Fluor 488/propidium iodide, as described by a Tali apoptosis kit (Life Technologies). Cell viability was evaluated using the Tali image-based cytometer (Life Technologies). The annexin V–positive cells were recognized as dead cells by the cytometer software and expressed as percentage of cellular death.

Subjects and housing

Animals used in all procedures were 10- to 19-week-old gut-corrected CFTR-deficient male C57BL/6 Cftrtm1UNCTgN(FABPCFTR)#Jaw mice (CFTR-KO) and their WT littermates. All mice were maintained under specific pathogen–free conditions in sterile cages, which were put into a ventilated isolator. Fluorescent lights were cycled 12 hours on and 12 hours off, and ambient temperature (23° ± 1°C) and relative humidity (40 to 60%) were regulated. Mice were fed with irradiated 5K-52 rodent chow (Safe, France) and autoclaved tap water.

Mouse model of chronic infection and lung histological analysis

For the infection procedure, *P. aeruginosa* AA43 strain isolated from a patient with CF before death was embedded in agar beads. Mice were anesthetized to implant into the lung an inoculum of 50 μl of agar bead suspension, embedding 1.5×10^6 CFU of AA43 strain.

Mice were treated with KB-R7943 (300 μg/kg) or vehicle via aerosol administration by Penn-Century MicroSprayer Aerosolizer every 12 hours starting 1 hour before infection. Two days after infection (1 hour after last treatment), mice were sacrificed to collect BALF and lungs for histopathological analysis. A detailed description of all the procedures used is reported in Supplementary Materials and Methods section.

Mass spectrometry

All the quantitative analysis of KB-R 7943 were performed using a Xevo TQD mass spectrometry instruments (Waters, USA) equipped with a Acquity ultraperformance liquid chromatography system with a BEH (ethylene bridged hybrid) C_{18} column using a linear gradient of water and acetonitrile with 0.1% of formic acid.

Cytokines assay

Airway epithelial cells were plated in six-well plates and left uninfected, pretreated with the selective inhibitor of caspase-1 [20 μM; 30 min before infection or KB-R7943 (1 μM) 1 hour before infection], and primed with bacteria (MOI of 100) for 6 hours at 37°C. IL-1β, TNFα, and IL-18 released in the cell culture supernatants and/or in

BALF were measured using an R&D Systems or an MBL enzyme-linked immunosorbent assay kit, respectively.

Statistical analysis and ethics statement

Unless otherwise indicated, all assays were performed independently and in triplicate, yielding comparable results. The data, which are presented as the means ± SE, were analyzed using Microsoft Excel (Microsoft Co.), and statistical significance was determined by Student's *t* tests and analysis of variance (ANOVA). Statistical analysis was performed with Prism (GraphPad Prism, USA) and Microsoft Excel (Microsoft Co). $^{**}P < 0.01$ and $^{*}P < 0.05$ were considered statistically significant.

This study was carried out according to protocols approved by San Raffaele Scientific Institute (Milan, Italy) Institutional Animal Care and Use Committee, in strict accordance with the recommendations in the *Guide for the Care and Use of Laboratory Animals* of the Italian Ministry of Health. The experimental protocol has been approved by the Italian Ministry of Health (protocol number 733).

SUPPLEMENTARY MATERIALS

Supplementary material for this article is available at http://advances.sciencemag.org/cgi/content/full/6/19/eaax9093/DC1

View/request a protocol for this paper from *Bio-protocol*.

REFERENCES AND NOTES

1. J. S. Elborn, Cystic fibrosis. *Lancet* **388**, 2519–2531 (2016).
2. L.-C. Tsui, R. Dorfman, The cystic fibrosis gene: A molecular genetic perspective. *Cold Spring Harb. Perspect. Med.* **3**, a009472 (2013).
3. E. A. Roesch, D. P. Nichols, J. F. Chmiel, Inflammation in cystic fibrosis: An update. *Pediatr. Pulmonol.* , (2018).
4. R. Rubino, V. Bezzerri, M. Favia, M. Facchini, M. Tebon, A. K. Singh, B. Riederer, U. Seidler, A. Iannucci, A. Bragonzi, G. Cabrini, S. J. Reshkin, A. Tamanini, *Pseudomonas aeruginosa* reduces the expression of CFTR via post-translational modification of NHERF1. *Pflugers Arch.* **466**, 2269–2278 (2014).
5. L. R. Hoffman, B. W. Ramsey, Cystic fibrosis therapeutics: The road ahead. *Chest* **143**, 207–213 (2013).
6. M. E. Martino, J. C. Olsen, N. B. Fulcher, M. C. Wolfgang, W. K. O'Neal, C. M. P. Ribeiro, Airway epithelial inflammation-induced endoplasmic reticulum Ca^{2+} store expansion is mediated by X-box binding protein-1. *J. Biol. Chem.* **284**, 14904–14913 (2009).
7. A. Rimessi, V. Bezzerri, S. Patergnani, S. Marchi, G. Cabrini, P. Pinton, Mitochondrial Ca^{2+}–dependent NLRP3 activation exacerbates the *Pseudomonas aeruginosa*-driven inflammatory response in cystic fibrosis. *Nat. Commun.* **6**, 6201 (2015).
8. M. W. Pellegrino, A. M. Nargund, N. V. Kirienko, R. Gillis, C. J. Fiorese, C. M. Haynes, Mitochondrial UPR-regulated innate immunity provides resistance to pathogen infection. *Nature* **516**, 414–417 (2014).
9. J. E. Irazoqui, E. R. Troemel, R. L. Feinbaum, L. G. Luhachack, B. O. Cezairliyan, F. M. Ausubel, Distinct pathogenesis and host responses during infection of *C. elegans by P. aeruginosa and S. aureus*. *PLOS Pathog.* **6**, e1000982 (2010).
10. A. Tosco, F. De Gregorio, S. Esposito, D. De Stefano, I. Sana, E. Ferrari, A. Sepe, L. Salvadori, P. Buonpensiero, A. Di Pasqua, R. Grassia, C. A. Leone, S. Guido, G. De Rosa, S. Lusa, G. Bona, G. Stoll, M. C. Maiuri, A. Mehta, G. Kroemer, L. Maiuri, V. Raia, A novel treatment of cystic fibrosis acting on-target: Cysteamine plus epigallocatechin gallate for the autophagy-dependent rescue of class II-mutated CFTR. *Cell Death Differ.* **23**, 1380–1393 (2016).
11. C. Cárdenas, R. A. Miller, I. Smith, T. Bui, J. Molgó, M. Müller, H. Vais, K.-H. Cheung, J. Yang, I. Parker, C. B. Thompson, M. J. Birnbaum, K. R. Hallows, J. K. Foskett, Essential regulation of cell bioenergetics by constitutive $InsP_3$ receptor Ca^{2+} transfer to mitochondria. *Cell* **142**, 270–283 (2010).
12. J.-P. Decuypere, G. Bultynck, J. B. Parys, A dual role for Ca^{2+} in autophagy regulation. *Cell Calcium* **50**, 242–250 (2011).
13. A. Rimessi, M. Bonora, S. Marchi, S. Patergnani, C. M. T. Marobbio, F. M. Lasorsa, P. Pinton, Perturbed mitochondrial Ca^{2+} signals as causes or consequences of mitophagy induction. *Autophagy* **9**, 1677–1686 (2013).
14. R. D. Junkins, A. Shen, K. Rosen, C. McCormick, T.-J. Lin, Autophagy enhances bacterial clearance during *P. aeruginosa* lung infection. *PlOS ONE* **8**, e72263 (2013).
15. A. Luciani, V. R. Villella, S. Esposito, N. Brunetti-Pierri, D. Medina, C. Settembre, M. Gavina, L. Pulze, I. Giardino, M. Pettoello-Mantovani, M. D'Apolito, S. Guido, E. Masliah, B. Spencer, S. Quaratino, V. Raia, A. Ballabio, L. Maiuri, Defective CFTR induces aggresome formation and lung inflammation in cystic fibrosis through ROS-mediated autophagy inhibition. *Nat. Cell Biol.* **12**, 863–875 (2010).
16. V. Bezzerri, P. d'Adamo, A. Rimessi, C. Lanzara, S. Crovella, E. Nicolis, A. Tamanini, E. Athanasakis, M. Tebon, G. Bisoffi, M. L. Drumm, M. R. Knowles, P. Pinton, P. Gasparini, G. Berton, G. Cabrini, Phospholipase C-β3 is a key modulator of IL-8 expression in cystic fibrosis bronchial epithelial cells. *J. Immunol.* **186**, 4946–4958 (2011).
17. P. Prandini, F. De Logu, C. Fusi, L. Provezza, R. Nassini, G. Montagner, S. Materazzi, S. Munari, E. Gilioli, V. Bezzerri, A. Finotti, I. Lampronti, A. Tamanini, M. C. Dechecchi, G. Lippi, C. M. Ribeiro, A. Rimessi, P. Pinton, R. Gambari, P. Geppetti, G. Cabrini, Transient receptor potential ankyrin 1 channels modulate inflammatory response in respiratory cells from patients with cystic fibrosis. *Am. J. Respir. Cell Mol. Biol.* **55**, 645–656 (2016).
18. C. M. P. Ribeiro, The role of intracellular calcium signals in inflammatory responses of polarised cystic fibrosis human airway epithelia. *Drugs R D* **7**, 17–31 (2006).
19. A. Rimessi, V. Bezzerri, F. Salvatori, A. Tamanini, F. Nigro, M. C. Dechecchi, A. Santangelo, P. Prandini, S. Munari, L. Provezza, N. Garreau de Loubresse, J. Muller, C. M. P. Ribeiro, G. Lippi, R. Gambari, P. Pinton, G. Cabrini, PLCB3 loss of function reduces *Pseudomonas aeruginosa*-dependent IL-8 release in cystic fibrosis. *Am. J. Respir. Cell Mol. Biol.* **59**, 428–436 (2018).
20. C. Giorgi, S. Marchi, P. Pinton, The machineries, regulation and cellular functions of mitochondrial calcium. *Nat. Rev. Mol. Cell Biol.* **19**, 713–730 (2018).
21. C. Giorgi, A. Danese, S. Missiroli, S. Patergnani, P. Pinton, Calcium dynamics as a machine for decoding signals. *Trends Cell Biol.* **28**, 258–273 (2018).
22. A. Rimessi, C. Giorgi, P. Pinton, R. Rizzuto, The versatility of mitochondrial calcium signals: From stimulation of cell metabolism to induction of cell death. *Biochim. Biophys. Acta* **1777**, 808–816 (2008).
23. S. Marchi, S. Patergnani, S. Missiroli, G. Morciano, A. Rimessi, M. R. Wieckowski, C. Giorgi, P. Pinton, Mitochondrial and endoplasmic reticulum calcium homeostasis and cell death. *Cell Calcium* **69**, 62–72 (2018).
24. C. Giorgi, S. Missiroli, S. Patergnani, J. Duszynski, M. R. Wieckowski, P. Pinton, Mitochondria-associated membranes: Composition, molecular mechanisms, and physiopathological implications. *Antioxid. Redox Signal.* **22**, 995–1019 (2015).
25. R. Stoica, K. J. De Vos, S. Paillusson, S. Mueller, R. M. Sancho, K.-F. Lau, G. Vizcay-Barrena, W.-L. Lin, Y.-F. Xu, J. Lewis, D. W. Dickson, L. Petrucelli, J. C. Mitchell, C. E. Shaw, C. C. J. Miller, ER-mitochondria associations are regulated by the VAPB-PTPIP51 interaction and are disrupted by ALS/FTD-associated TDP-43. *Nat. Commun.* **5**, 3996 (2014).
26. P. Gomez-Suaga, S. Paillusson, R. Stoica, W. Noble, D. P. Hanger, C. C. J. Miller, The ER-Mitochondria Tethering Complex VAPB-PTPIP51 Regulates Autophagy. *Curr. Biol.* **27**, 371–385 (2017).
27. M. Lazarou, D. A. Sliter, L. A. Kane, S. A. Sarraf, C. Wang, J. L. Burman, D. P. Sideris, A. I. Fogel, R. J. Youle, The ubiquitin kinase PINK1 recruits autophagy receptors to induce mitophagy. *Nature* **524**, 309–314 (2015).
28. R. Garcia-Medina, W. M. Dunne, P. K. Singh, S. L. Brody, *Pseudomonas aeruginosa* acquires biofilm-like properties within airway epithelial cells. *Infect. Immun.* **73**, 8298–8305 (2005).
29. C. J. Fiorese, A. M. Schulz, Y.-F. Lin, N. Rosin, M. W. Pellegrino, C. M. Haynes, The Transcription Factor ATF5 Mediates a Mammalian Mitochondrial UPR. *Curr. Biol.* **26**, 2037–2043 (2016).
30. Z. Sheng, L. Ma, J. E. Sun, L. J. Zhu, M. R. Green, BCR-ABL suppresses autophagy through ATF5-mediated regulation of *mTOR* transcription. *Blood* **118**, 2840–2848 (2011).
31. J. Santo-Domingo, L. Vay, E. Hernández-SanMiguel, C. D. Lobatón, A. Moreno, M. Montero, J. Alvarez, The plasma membrane Na^+/Ca^{2+} exchange inhibitor KB-R7943 is also a potent inhibitor of the mitochondrial Ca^{2+} uniporter. *Br. J. Pharmacol.* **151**, 647–654 (2007).
32. A. Zsembery, J. A. Fortenberry, L. Liang, Z. Bebok, T. A. Tucker, A. T. Boyce, G. M. Braunstein, E. Welty, P. D. Bell, E. J. Sorscher, J. P. Clancy, E. M. Schwiebert, Extracellular zinc and ATP restore chloride secretion across cystic fibrosis airway epithelia by triggering calcium entry. *J. Biol. Chem.* **279**, 10720–10729 (2004).
33. T. Brustovetsky, M. K. Brittain, P. L. Sheets, T. R. Cummins, V. Pinelis, N. Brustovetsky, KB-R7943, an inhibitor of the reverse Na^+/Ca^{2+} exchanger, blocks N-methyl-D-aspartate receptor and inhibits mitochondrial complex I. *Br. J. Pharmacol.* **162**, 255–270 (2011).
34. T. P. Storozhevykh, Y. E. Senilova, T. Brustovetsky, V. G. Pinelis, N. Brustovetsky, Neuroprotective effect of KB-R7943 against glutamate excitotoxicity is related to mild mitochondrial depolarization. *Neurochem. Res.* **35**, 323–335 (2010).
35. B. M. Wiczer, R. Marcu, B. J. Hawkins, KB-R7943, a plasma membrane Na^+/Ca^{2+} exchanger inhibitor, blocks opening of the mitochondrial permeability transition pore. *Biochem. Biophys. Res. Commun.* **444**, 44–49 (2014).
36. K. B. Hisert, S. L. Heltshe, C. Pope, P. Jorth, X. Wu, R. M. Edwards, M. Radey, F. J. Accurso, D. J. Wolter, G. Cooke, R. J. Adam, S. Carter, B. Grogan, J. L. Launspach, S. C. Donnelly, C. G. Gallagher, J. E. Bruce, D. A. Stoltz, M. J. Welsh, L. R. Hoffman, E. F. McKone, P. K. Singh, Restoring cystic fibrosis transmembrane conductance regulator function reduces airway

bacteria and inflammation in people with cystic fibrosis and chronic lung infections. *Am. J. Respir. Crit. Care Med.* **195**, 1617–1628 (2017).
37. M. A. Puertollano, E. Puertollano, G. A. de Cienfuegos, M. A. de Pablo, Dietary antioxidants: Immunity and host defense. *Curr. Top. Med. Chem.* **11**, 1752–1766 (2011).
38. R. Zhou, A. S. Yazdi, P. Menu, J. Tschopp, A role for mitochondria in NLRP3 inflammasome activation. *Nature* **469**, 221–225 (2011).
39. N. V. Kirienko, F. M. Ausubel, G. Ruvkun, Mitophagy confers resistance to siderophore-mediated killing by *Pseudomonas aeruginosa*. *Proc. Natl. Acad. Sci. U.S.A.* **112**, 1821–1826 (2015).
40. M. A. Qureshi, C. M. Haynes, M. W. Pellegrino, The mitochondrial unfolded protein response: Signaling from the powerhouse. *J. Biol. Chem.* **292**, 13500–13506 (2017).
41. M. Bonora, S. Patergnani, A. Rimessi, E. De Marchi, J. M. Suski, A. Bononi, C. Giorgi, S. Marchi, S. Missiroli, F. Poletti, M. R. Wieckowski, P. Pinton, ATP synthesis and storage. *Purinergic Signal* **8**, 343–357 (2012).
42. S. Böckler, B. Westermann, Mitochondrial ER contacts are crucial for mitophagy in yeast. *Dev. Cell* **28**, 450–458 (2014).
43. K. Mallilankaraman, C. Cárdenas, P. J. Doonan, H. C. Chandramoorthy, K. M. Irrinki, T. Golenár, G. Csordás, P. Madireddi, J. Yang, M. Müller, R. Miller, J. E. Kolesar, J. Molgó, B. Kaufman, G. Hajnóczky, J. K. Foskett, M. Madesh, MCUR1 is an essential component of mitochondrial Ca^{2+} uptake that regulates cellular metabolism. *Nat. Cell Biol.* **14**, 1336–1343 (2012).
44. M. A. Rodgers, J. W. Bowman, Q. Liang, J. U. Jung, Regulation where autophagy intersects the inflammasome. *Antioxid. Redox Signal.* **20**, 495–506 (2014).
45. M. Takahama, S. Akira, T. Saitoh, Autophagy limits activation of the inflammasomes. *Immunol. Rev.* **281**, 62–73 (2018).
46. D. M. Arduino, J. Wettmarshausen, H. Vais, P. Navas-Navarro, Y. Cheng, A. Leimpek, Z. Ma, A. Delrio-Lorenzo, A. Giordano, C. Garcia-Perez, G. Médard, B. Kuster, J. García-Sancho, D. Mokranjac, J. K. Foskett, M. T. Alonso, F. Perocchi, Systematic Identification of MCU Modulators by Orthogonal Interspecies Chemical Screening. *Mol. Cell* **67**, 711–723.e7 (2017).
47. T. Iwamoto, T. Watano, M. Shigekawa, A novel isothiourea derivative selectively inhibits the reverse mode of Na^+/Ca^{2+} exchange in cells expressing NCX1. *J. Biol. Chem.* **271**, 22391–22397 (1996).
48. H. Hagihara, Y. Yoshikawa, Y. Ohga, C. Takenaka, K.-Y. Murata, S. Taniguchi, M. Takaki, Na^+/Ca^{2+} exchange inhibition protects the rat heart from ischemia-reperfusion injury by blocking energy-wasting processes. *Am. J. Physiol. Heart Circ. Physiol.* **288**, H1699–H1707 (2005).
49. M. Matsunaga, M. Saotome, H. Satoh, H. Katoh, H. Terada, H. Hayashi, Different actions of cardioprotective agents on mitochondrial Ca^{2+} regulation in a Ca^{2+} paradox-induced Ca^{2+} overload. *Circ. J.* **69**, 1132–1140 (2005).
50. T. Iwamoto, S. Kita, A. Uehara, Y. Inoue, Y. Taniguchi, I. Imanaga, M. Shigekawa, Structural domains influencing sensitivity to isothiourea derivative inhibitor KB-R7943 in cardiac Nna^+/Ca^{2+} exchanger. *Mol. Pharmacol.* **59**, 524–531 (2001).
51. A. Scorziello, C. Savoia, M. J. Sisalli, A. Adornetto, A. Secondo, F. Boscia, A. Esposito, E. V. Polishchuk, R. S. Polishchuk, P. Molinaro, A. Carlucci, L. Lignitto, G. Di Renzo, A. Feliciello, L. Annunziato, NCX3 regulates mitochondrial Ca^{2+} handling through the AKAP121-anchored signaling complex and prevents hypoxia-induced neuronal death. *J. Cell Sci.* **126**, 5566–5577 (2013).
52. M. S. Amran, N. Homma, K. Hashimoto, Pharmacology of KB-R7943: A Na^+-Ca^{2+} exchange inhibitor. *Cardiovasc. Drug Rev.* **21**, 255–276 (2003).
53. F. Schweda, H. Seebauer, B. K. Krämer, A. Kurtz, Functional role of sodium-calcium exchange in the regulation of renal vascular resistance. *Am. J. Physiol. Renal Physiol.* **280**, F155–F161 (2001).
54. Z. Long, B. Chen, Q. Liu, J. Zhao, Z. Yang, X. Dong, L. Xia, S. Huang, X. Hu, B. Song, L. Li, The reverse-mode NCX1 activity inhibitor KB-R7943 promotes prostate cancer cell death by activating the JNK pathway and blocking autophagic flux. *Oncotarget* **7**, 42059–42070 (2016).
55. C. A. Hobbs, C. Da Tan, R. Tarran, Does epithelial sodium channel hyperactivity contribute to cystic fibrosis lung disease? *J. Physiol.* **591**, 4377–4387 (2013).
56. B. Liu, S. E. Peel, J. Fox, I. P. Hall, Reverse mode Na^+/Ca^{2+} exchange mediated by STIM1 contributes to Ca^{2+} influx in airway smooth muscle following agonist stimulation. *Respir. Res.* **11**, 168 (2010).
57. A. Criollo, M. C. Maiuri, E. Tasdemir, I. Vitale, A. A. Fiebig, D. Andrews, J. Molgó, J. Díaz, S. Lavandero, F. Harper, G. Pierron, D. di Stefano, R. Rizzuto, G. Szabadkai, G. Kroemer, Regulation of autophagy by the inositol trisphosphate receptor. *Cell Death Differ.* **14**, 1029–1039 (2007).
58. P. B. Gordon, I. Holen, M. Fosse, J. S. Røtnes, P. O. Seglen, Dependence of hepatocytic autophagy on intracellularly sequestered calcium. *J. Biol. Chem.* **268**, 26107–26112 (1993).
59. A. Rimessi, M. Previati, F. Nigro, M. R. Wieckowski, P. Pinton, Mitochondrial reactive oxygen species and inflammation: Molecular mechanisms, diseases and promising therapies. *Int. J. Biochem. Cell Biol.* **81**, 281–293 (2016).
60. C. Loriol, S. Dulong, M. Avella, N. Gabillat, K. Boulukos, F. Borgese, J. Ehrenfeld, Characterization of SLC26A9, facilitation of Cl^- transport by bicarbonate. *Cell. Physiol. Biochem.* **22**, 15–30 (2008).
61. M. Facchini, I. De Fino, C. Riva, A. Bragonzi, Long term chronic *Pseudomonas aeruginosa* airway infection in mice. *J. Vis. Exp.*, e51019 (2014).
62. A. Cersini, M. C. Martino, I. Martini, G. Rossi, M. L. Bernardini, Analysis of virulence and inflammatory potential of *Shigella flexneri* purine biosynthesis mutants. *Infect. Immun.* **71**, 7002–7013 (2003).
63. M. C. Martino, G. Rossi, I. Martini, I. Tattoli, D. Chiavolini, A. Phalipon, P. J. Sansonetti, M. L. Bernardini, Mucosal lymphoid infiltrate dominates colonic pathological changes in murine experimental shigellosis. *J. Infect. Dis.* **192**, 136–148 (2005).
64. M. J. Dykstra, S. Levisohn, O. J. Fletcher, S. H. Kleven, Evaluation of cytopathologic changes induced in chicken tracheal epithelium by Mycoplasma gallisepticum in vivo and in vitro. *Am. J. Vet. Res.* **46**, 116–122 (1985).

Acknowledgments: We are grateful to C. C. J. Miller (King's College London), P. Pizzo, and T. Pozzan (University of Padua) for HA-tagged PTPIP51 and Myc-tagged VAPB cDNA; C. M. Haynes (University of Massachusetts) for ATF5 in pEGFP plasmid; and B. Tümmler (Medizinische Hochschule Hannover) for supplying the *P. aeruginosa* AA43 clinical isolate. **Funding:** This study was supported initially by the Italian Cystic Fibrosis Research Foundation (grant FFC no. 19/2014 to P.P., FFC no. 20/2015 to A.R., and CFaCore to A.B.). Moreover, the Signal Transduction Laboratory is supported by the following: the local founds from University of Ferrara, FIR-2017, the Italian Ministry of Health (GR-2016-02364602), and the Italian Ministry of Education, University and Research (PRIN grant 2017XA5J5N) to A.R. and the Italian Association for Cancer Research (AIRC, IG-23670), Telethon (GGP11139B), local funds from the University of Ferrara, and the Italian Ministry of Education, University and Research (PRIN grant 2017E5L5P3) to P.P. M.R.W. was supported by the Polish National Science Centre (grant UMO-2014/15/NZ1/00490). P.P. is grateful to C. d. Scrovegni for continuous support.
Author contributions: A.Ri. and P.P. designed the experiments. A.Ri., C.P., and L.C. carried out most of the experiments and data analysis. A.B., A.Ro., S.R., I.D.F., and C.C. performed the experiments in vivo, while the histopathological analysis was performed by G.R. C.T. and A.T. performed the drug distribution analysis. A.Ri., A.B., C.M.P.R., M.R.W., G.C., and P.P. contributed to the interpretation and discussion of results. A.Ri. and P.P. wrote the manuscript with input from all authors. **Competing interests:** The authors declare that they have no competing interests. **Data and materials availability:** All data needed to evaluate the conclusions in the paper are present in the paper and/or in the Supplementary Materials. Additional data related to this paper may be requested from the authors.

Submitted 6 May 2019
Accepted 20 February 2020
Published 6 May 2020
10.1126/sciadv.aax9093

Citation: A. Rimessi, C. Pozzato, L. Carparelli, A. Rossi, S. Ranucci, I. De Fino, C. Cigana, A. Talarico, M. R. Wieckowski, C. M. P. Ribeiro, C. Trapella, G. Rossi, G. Cabrini, A. Bragonzi, P. Pinton, Pharmacological modulation of mitochondrial calcium uniporter controls lung inflammation in cystic fibrosis. *Sci. Adv.* **6**, eaax9093 (2020).

Pharmacological modulation of mitochondrial calcium uniporter controls lung inflammation in cystic fibrosis

Alessandro Rimessi, Chiara Pozzato, Lorenzo Carparelli, Alice Rossi, Serena Ranucci, Ida De Fino, Cristina Cigana, Anna Talarico, Mariusz R. Wieckowski, Carla M. P. Ribeiro, Claudio Trapella, Giacomo Rossi, Giulio Cabrini, Alessandra Bragonzi and Paolo Pinton

Sci Adv **6** (19), eaax9093.
DOI: 10.1126/sciadv.aax9093

Science Advances
AAAS

advances.sciencemag.org/cgi/content/full/6/19/eaax9093/DC1

Supplementary Materials for

Pharmacological modulation of mitochondrial calcium uniporter controls lung inflammation in cystic fibrosis

Alessandro Rimessi*, Chiara Pozzato, Lorenzo Carparelli, Alice Rossi, Serena Ranucci, Ida De Fino, Cristina Cigana, Anna Talarico, Mariusz R. Wieckowski, Carla M. P. Ribeiro, Claudio Trapella, Giacomo Rossi, Giulio Cabrini, Alessandra Bragonzi, Paolo Pinton*

*Corresponding author. Email: alessandro.rimessi@unife.it (A.R.); paolo.pinton@unife.it (P.P.)

Published 6 May 2020, *Sci. Adv.* **6**, eaax9093 (2020)
DOI: 10.1126/sciadv.aax9093

This PDF file includes:

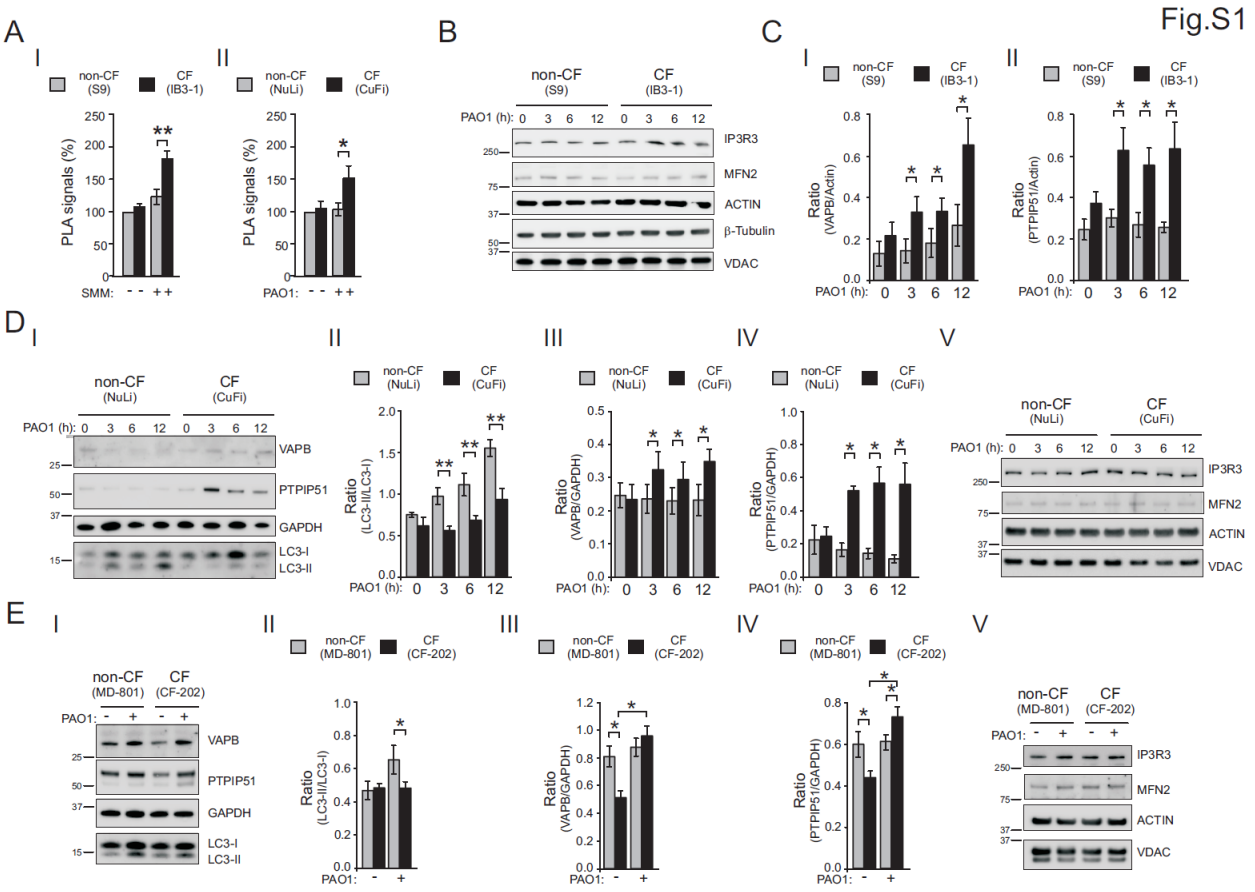

Supplementary figure 1: ***Defective CFTR channel favors ER-mitochondria interaction during pathogen infection in CF bronchial cells.***

A) The bar chart shows quantification of PLA signals (%) for IP3R3 and VDAC interactions (I) in S9 (non-CF) and IB3-1 (CF) cells exposed to supernatant from mucopurulent material from CF patients (SMM); (II) in NuLi (non-CF) and CuFi (CF) cells infected with PAO1 at 100 MOI for 6 hours. The bar chart shows quantification of PLA signals (%), respect to uninfected non-CF cells (n=25-35 independent visual field for each condition of three independent experiments). **B**) Immunoblots show ER-mitochondria Ca^{2+} exchange proteins and tethers expression in S9 (non-CF) and IB3-1 (CF) cells during *P. aeruginosa* infection. The samples were probed using the antibodies indicated, where actin and β-tubulin are used as loading control. **C**) Western blot quantification, expressed as the ratio of VAPB/actin (I) and PTPIP51/actin (II), of the blot in figure 1B, as previously described (n=5-6 of independent experiments). **D**) (I) Immunoblots show VAPB and PTPIP51 expression in NuLi (non-CF) and CuFi (CF) cells during *P. aeruginosa* infection. The cells were uninfected or infected with PAO1 at 100 MOI for three, six and twelve hours. The samples were probed using the antibodies indicated, where GAPDH is used as loading control. Protein molecular mass markers are indicated in kD. (II) Bar chart shows the ratio LC3-II/LC3-I, (III) the ratio of VAPB/GAPDH and (IV) PTPIP51/GAPDH following quantification of signals from immunoblots (n=3); (V) Immunoblots show ER-mitochondria Ca^{2+} exchange proteins and tethers expression in NuLi (non-CF) and CuFi (CF) cells during *P. aeruginosa* infection. The samples were probed using the antibodies indicated, where actin is used as loading control. **E**) (I)

Immunoblots show VAPB and PTPIP51 expression in polarized mucociliary-differentiated donor-derived airway cells (MD-801, non-CF) and ΔF508/F508 patient-derived airway cells (CF-202, CF) during *P. aeruginosa* infection. The cells were uninfected or infected with PAO1 at 100 MOI for six hours. The samples were probed using the antibodies indicated, where GAPDH is used as loading control. Protein molecular mass markers are indicated in kD. (II) Bar chart shows the ratio of LC3-II/LC3-I, (III) of VAPB/GAPDH and (IV) of PTPIP51/GAPDH following quantification of signals from immunoblots (n=3); (V) Immunoblots show ER-mitochondria Ca^{2+} exchange proteins and tethers expression in polarized mucociliary-differentiated donor-derived airway cells (MD-801, non-CF) and ΔF508/F508 patient-derived airway cells (CF-202, CF) during *P. aeruginosa* infection. The samples were probed using the antibodies indicated, where actin is used as loading control. *t*-Test used for indicated comparisons (* $p<0.05$ and ** $p<0.01$).

Fig.S2

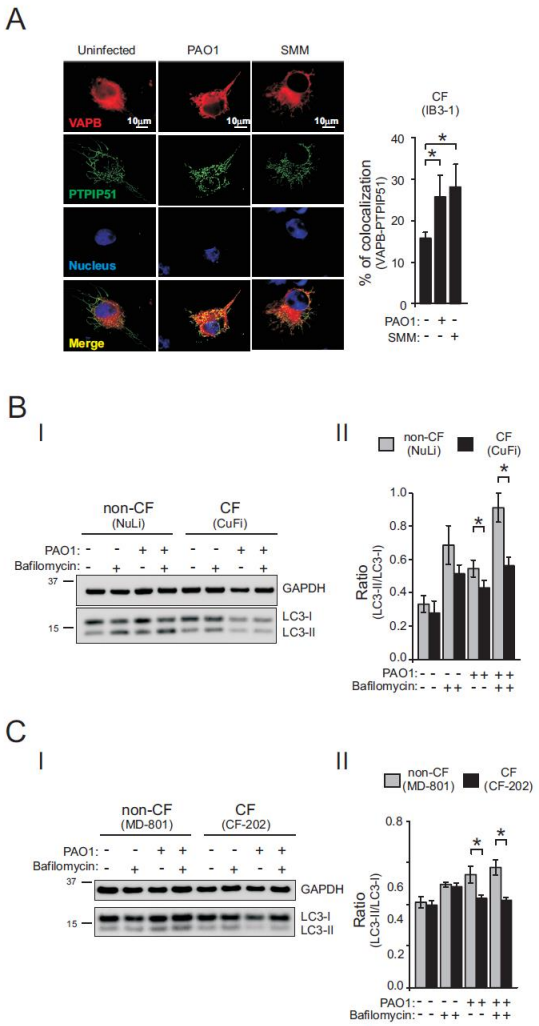

Supplementary figure 2: ***The downregulation of autophagy in CF bronchial cells is the consequence of the enhanced ER-mitochondria interaction during P. aeruginosa.***

A) Confocal immunofluorescence images of IB3-1 cells cotransfected with Myc-VAPB and Ha-PTPIP51. The cells were probed using respectively Myc-tag and Ha-tag primary antibodies. Colocalization of VAPB and PTPIP51 signal during PAO1 (100 MOI) or SMM (1:100) exposition was performed and expressed as the % of colocalization, which was calculated as average volume of the overlapping areas (n=8 independent visual field for each condition). **B**) NuLi (non-CF) and CuFi (CF) cells were infected with PAO1 at 100 MOI for 6 hours and then treated with either vehicle or bafilomycin A1 (100nM) as indicated. (I) The samples were probed on immunoblots for LC3 and GAPDH as a loading control. (II) Bar chart shows the ratio LC3-II/LC3-I following quantification of signals from immunoblots (n=6). **C**) Polarized mucociliary-differentiated donor-derived airway cells (MD-801, non-CF) and ΔF508/F508 patient-derived airway cells (CF-202, CF) were infected with PAO1 at 100 MOI for 6 hours and then treated with either vehicle or bafilomycin A1 (100nM) as indicated. (I) The samples were probed on immunoblots for LC3 and GAPDH as a loading control. (II) Bar chart shows the ratio LC3-II/LC3-I following quantification of signals from immunoblots (n=6). *t*-Test used for indicated comparisons (* $p<0.05$ and ** $p<0.01$).

Fig.S3

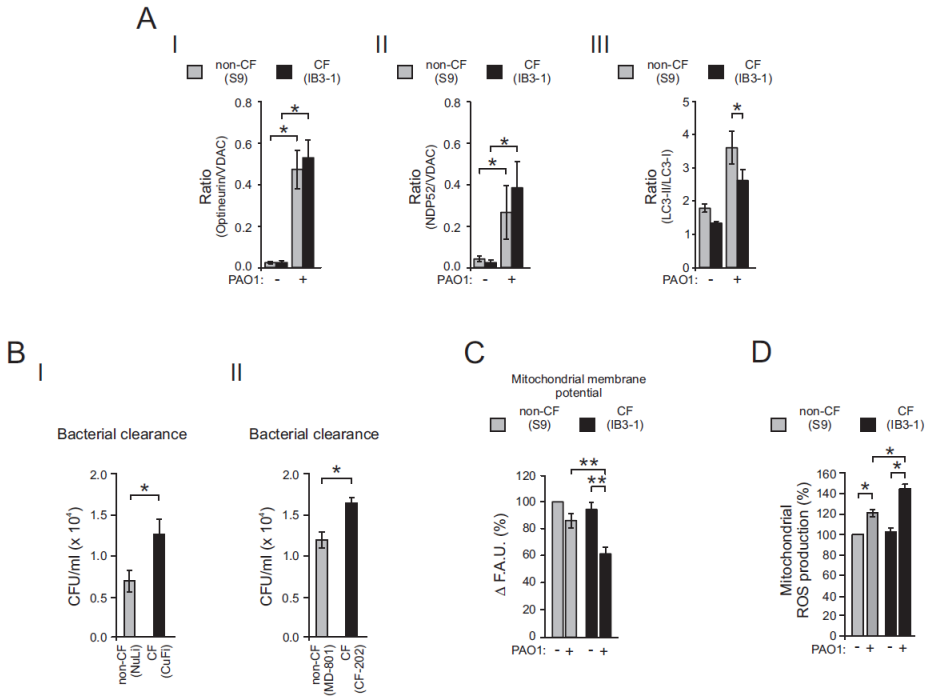

Supplementary figure 3: ***Defective CFTR channel lead to down regulation of xenophagy and mitophagy in CF bronchial cells.***

A) Western blot quantification of mitophagic markers in mitochondrial fraction, expressed as the ratio of (I) Optineurin/VDAC, (II) NDP52/VDAC and (III) LC3-II/LC3-I of the blot in figure 2A, as previously described (n=4 of independent experiments). **B**) *P. aeruginosa*-infected (I) NuLi (non-CF) and CuFi (CF) cells or (II) Polarized mucociliary-differentiated donor-derived airway cells (MD-801, non-CF) and ΔF508/F508 patient-derived airway cells (CF-202, CF) were lysed after the addition of impermeable antibiotics and streaked on LB agar plates for the determination of intracellular CFUs (n=6 of independent experiments). **C**) Measurements of ΔΨ in S9 (non-CF) and IB3-1 (CF) cells after 6 hours of bacterial infection. The bars show the change in TMRM fluorescence level, expressed as % change with respect to S9 uninfected cells. FCCP was used to collapse the mitochondrial ΔΨ (n=12-20 of independent experiments). F.a.u., fluorescent arbitrary units. **D**) Effects of *P. aeruginosa* infection on mitochondrial superoxide production in S9 and IB3-1 cells. The quantification of % change of cells positive for MitoSox staining is shown (n=5-8 of independent experiments). *t*-Test used for indicated comparisons (* $p<0.05$ and ** $p<0.01$).

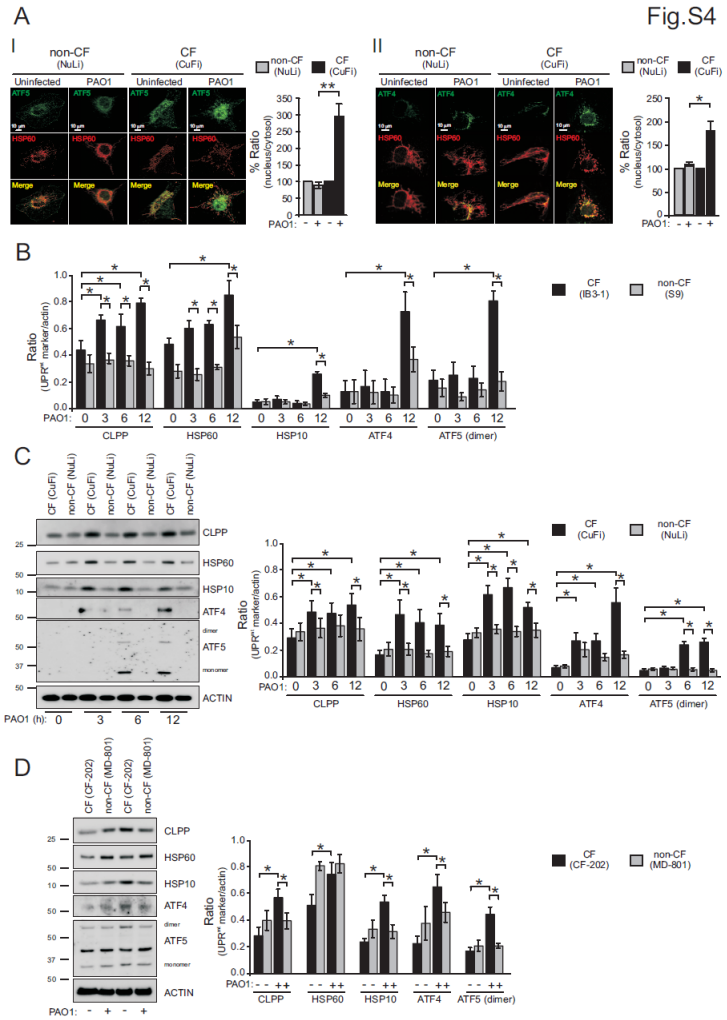

Supplementary figure 4: ***Defective CFTR channel lead a persistent activation of UPR^{mt} in CF bronchial cells during pathogen infection.***

A) Representative confocal images of nuclear translocation of endogenous ATF5 (I) and ATF4 (II) in NuLi (non-CF) and CuFi (CF) cells during pathogen infection. The graphs report the nuclear redistribution of ATF5 and ATF4 after PAO1 infection, expressed as percentage increase in fluorescent ratio signals (from cytosol to nucleus) with respect to uninfected condition (n=15 independent visual field for each condition of three independent experiments). **B**) Western blot quantification of UPR^{mt} markers, expressed as the ratio of CLPP/actin, HSP60/actin, HSP10/actin, ATF4/actin and ATF5 dimer/actin of the blot in figure 3B, as previously described (n=3 of independent experiments). **C**) Immunoblots of CuFi and NuLi cells uninfected or infected for three, six and twelve hours, as indicated. The samples were probed using the antibodies indicated, related to UPR^{mt} markers, where actin is used as loading control. Bar chart reports western blot quantification of UPR^{mt} markers, expressed as the ratio of CLPP/actin, HSP60/actin, HSP10/actin, ATF4/actin and ATF5 dimer/actin (n=4 of independent experiments). **D**) Immunoblots of polarized mucociliary-differentiated ΔF508/F508 patient-derived airway cells (CF-202, CF) and donor-derived airway cells (MD-801, non-CF) uninfected or infected for six hours. The samples were probed using the antibodies indicated, related to UPR^{mt} markers, where actin is used as loading control. Bar chart reports western blot quantification of UPR^{mt} markers, expressed as the ratio of CLPP/actin, HSP60/actin, HSP10/actin, ATF4/actin and ATF5 dimer/actin (n=3 of independent experiments). *t*-Test used for indicated comparisons (* $p<0.05$ and ** $p<0.01$).

Fig.S5

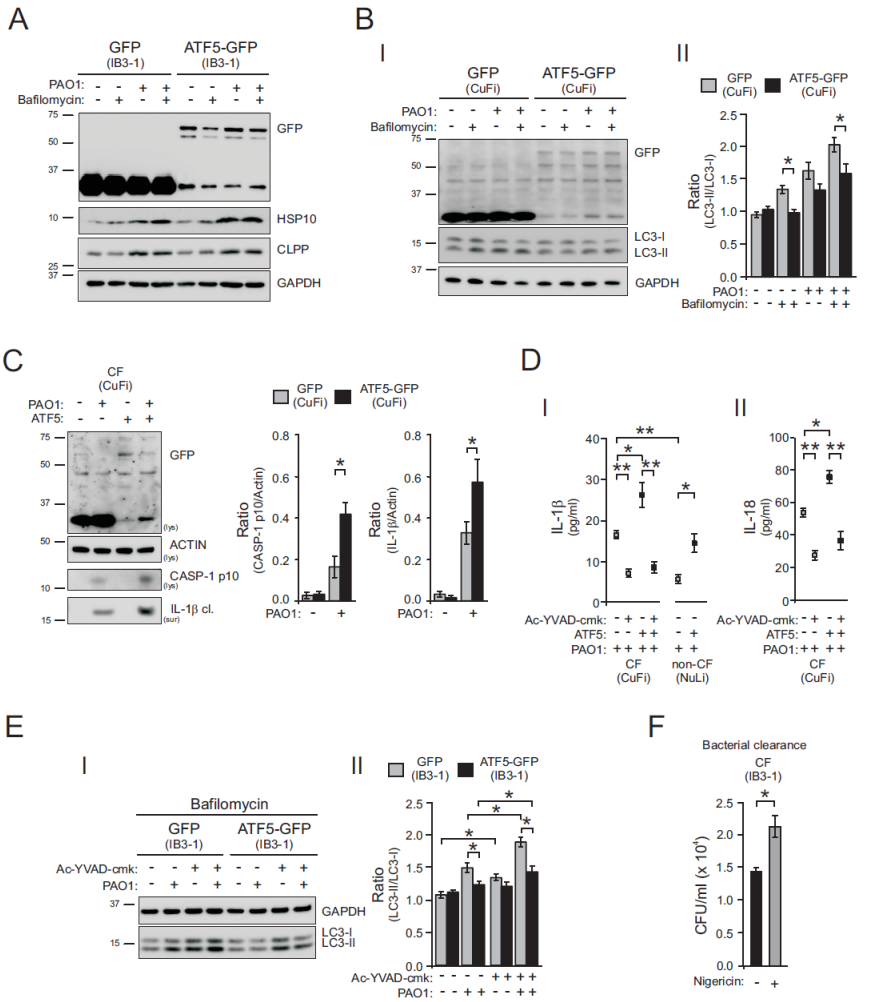

Supplementary figure 5: ***ATF5 potentiates the autophagic defect and the inflammasome response in CF bronchial cells during pathogen infection.***

A) The IB3-1 cells (CF) were transfected with GFP- and ATF5GFP and then infected with PAO1 at 100 MOI for six hours and successively treated with bafilomycin A1, as reported for figure 3C. The samples were probed using the antibodies indicated, where GAPDH is used as loading control. **B**) (I) Autophagic flux in CuFi cells (CF) overexpressing ATF5 during *P. aeruginosa* infection. GFP- and ATF5GFP-transfected cells were infected with PAO1 at 100 MOI for six hours and then treated with bafilomycin A1, as indicated. (II) Bar chart shows the ratio LC3-II/LC3-I following quantification of signals from immunoblots (n=4). **C**) Immunoblots of cleaved caspase-1 and processed IL-1β from lysates (lys) or supernatants (sur) of CuFi and ATF5-overexpressed CuFi cells infected for 6 hours with *P. aeruginosa*. Actin was used as loading control. The quantification is expressed as the ratio of casp1-p10/actin and IL-1β cl./actin. The bars are the means±SE of three independent immunoblots. **D**) Effects of ATF5 overexpression on the IL-1β (I) and IL-18 (II) release. NuLi (non-CF) and CuFi (CF) cells were transfected with ATF5-GFP and after 6 hours of PAO1 infection, the cultured cell supernatant were collected to quantify the levels of proinflammatory cytokines (n=8 of independent experiments). The selective inhibitor of caspase-1, Ac-YVAD-cmk 20μM, was added thirty minutes before infection. **E**) (I) Autophagic flux in

untreated and Ac-YVAD-cmk-treated IB3-1 cells (CF) overexpressing ATF5 during *P. aeruginosa* infection. GFP- and ATF5GFP-transfected cells were pre-treated with Ac-YVAD-cmk 20μM thirty minutes before infection with PAO1 at 100 MOI for six hours and successively treated with bafilomycin A1, as indicated. (II) Bar chart shows the ratio LC3-II/LC3-I following quantification of signals from immunoblots (n=4). **F**) Nigericin (10μM, thirty minutes before infection) treatment in IB3-1 cells affected the bacterial clearance of *P. aeruginosa*. Nigericin-treated and untreated IB3-1 cells were lysed after the addition of impermeable antibiotics and streaked on LB agar plates for the determination of intracellular *P. aeruginosa* CFUs (n=8 of independent experiments). *t*-Test used for indicated comparisons (* $p<0.05$ and ** $p<0.01$).

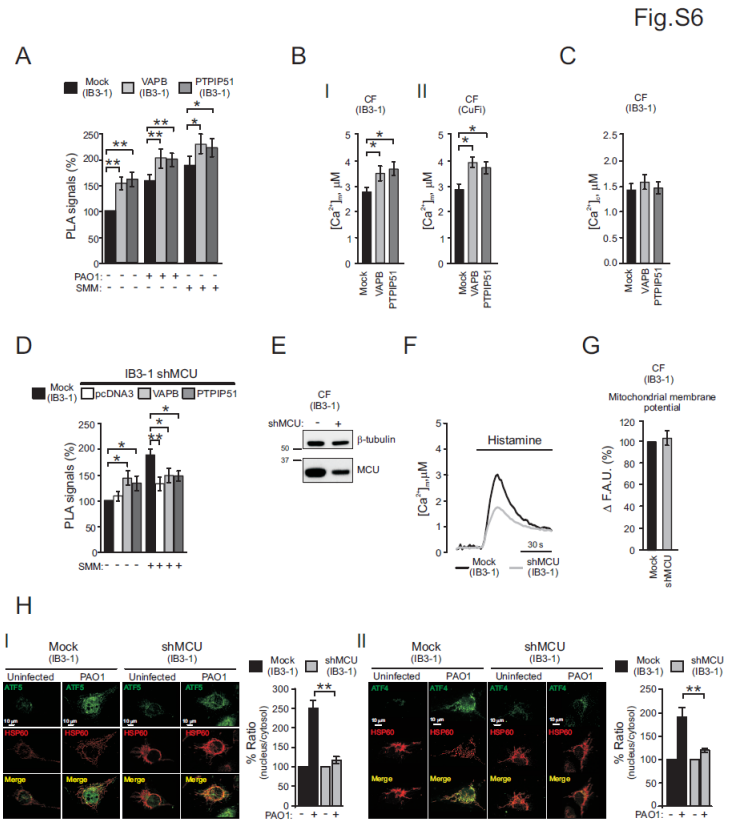

Supplementary figure 6: ***The silencing of MCU prevents the increase in ER-mitochondria interaction and the UPR^{mt} activation in CF bronchial cells exposed to pathogen.***

A) VAPB or PTPIP51 overexpression increases the IP3R3-VDAC interactions in IB3-1 cells. The bar chart shows quantification of PLA signals (%) respect to uninfected mock IB3-1 cells (n=15 independent visual field for each condition of three independent experiments). **B**) Histamine-dependent mitochondrial Ca^{2+} responses of mock-, VAPB- and PTPIP51-overexpressing IB3-1 (I) and CuFi (II) cells; (**C**) Histamine-dependent cytosolic Ca^{2+} responses of mock-, VAPB- and PTPIP51-overexpressing IB3-1 cells. The histograms show the mean±SE of mitochondrial and cytosolic Ca^{2+} responses (n=10-15 of independent experiments). **D**) The bar chart shows quantification of PLA signals (%) for IP3R3 and VDAC interactions in MCU-silenced (IB3-1 shMCU) and IB3-1 cells challenged with SMM. Stable MCU-silenced CF clone was transfected with control empty vector (mock), VAPB, or PTPIP51, then exposed to SMM (1:100) for 6 hours (n=15 independent visual field for each condition of three independent experiments). **E**) Endogenous level of MCU expression in stable MCU-silenced and IB3-1 cells. Cell lysates were immunoblotted with anti-MCU and anti-β tubulin as loading control. **F**) Representative measurements of histamine-induced mitochondrial Ca^{2+} response in MCU-silenced and IB3-1 cells. Cells were transfected with mitochondrial-targeted aequorin and stimulated with 100μM histamine to induce ER-mitochondria Ca^{2+} transfer. **G**) TMRM fluorescent measurements in MCU-silenced (shMCU) and IB3-1 cells in resting condition. The histograms show the % change of $\Delta\Psi$ in MCU-silenced IB3-1 cells compared to mock IB3-1 cells (n=12 of independent experiments). **H**)

Representative confocal images of nuclear translocation of endogenous ATF5 (I) and ATF4 (II) in IB3-1 (mock) and MCU-silenced IB3-1 (shMCU) cells during pathogen infection. The graphs report the nuclear redistribution of ATF5 and ATF4 after PAO1 infection, expressed as percentage increase in fluorescent ratio signals (from cytosol to nucleus) with respect to uninfected condition (n=15 independent visual field for each condition of three independent experiments). *t*-Test used for indicated comparisons (* $p<0.05$ and ** $p<0.01$).

Fig.S7

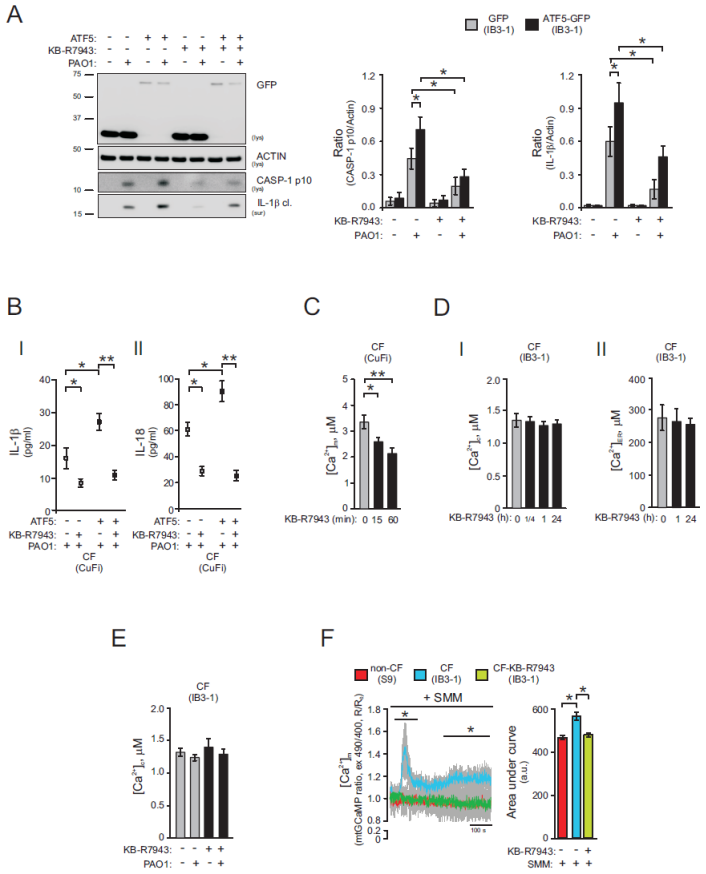

Supplementary figure 7: ***KB-R7943 prevents mitochondrial Ca^{2+} overload and inflammasome activation in CF bronchial cells during pathogen infection.***

A) Immunoblots of cleaved caspase-1 and processed IL-1β from lysates (lys) or supernatants (sur) of IB3-1 and ATF5-overexpressed IB3-1 cells, previously pretreated with MCU-inhibitor, KB-R7943 (1μM) for one hour then infected for 6 hours with *P. aeruginosa*. Actin was used as loading control. The quantification is expressed as the ratio of casp1-p10/actin and IL-1β cl./actin. The bars are the means±SE of four independent immunoblots. **B**) Effects of the pretreatment with KB-R7943 (1μM) on the levels of released IL-1β and IL-18 in mock and ATF5-overexpressing CuFi cells, collected after 6 hours of PAO1 infection at 100 MOI (n=8 of independent experiments). **C**) Histamine-dependent mitochondrial Ca^{2+} responses of KB-R7943 pretreating CuFi cells at different time points. The histograms show all mean±SE of mitochondrial Ca^{2+} responses (n=8 of independent experiments). **D**) No changes in histamine-induced cytosolic Ca^{2+} response (I) and intraluminal ER Ca^{2+} content (II) in IB3-1 cells exposed to MCU-inhibitor at different time points, as indicated. Before exposition, the cells were transfected with native and ER-targeted aequorin. The histograms show the mean value±SE (n=12-15 of independent experiments). **E**) Histamine-induced cytosolic Ca^{2+} response in IB3-1 cells treated with KB-R7943 and PAO1 at 100 MOI. **F**) Mitochondrial Ca^{2+} dynamics in S9 (non-CF), IB3-1 (CF) and KB-R7943-treated IB3-1 (CF-KB-R7943) cells exposed to SMM, evaluated through ratiometric imaging of mitochondrial targeted GCaMP6. Traces represent mean±SE of mitochondrial Ca^{2+} response from at least of 10 independent experiments. SE values are illustrated using grey shading. For statistical significance

the Multiple *t*-Test has been used. The bar chart shows the quantification of the area under the curve; a. u., arbitrary unit. *t*-Test used for indicated comparisons (* $p<0.05$ and ** $p<0.01$).

Fig.S8

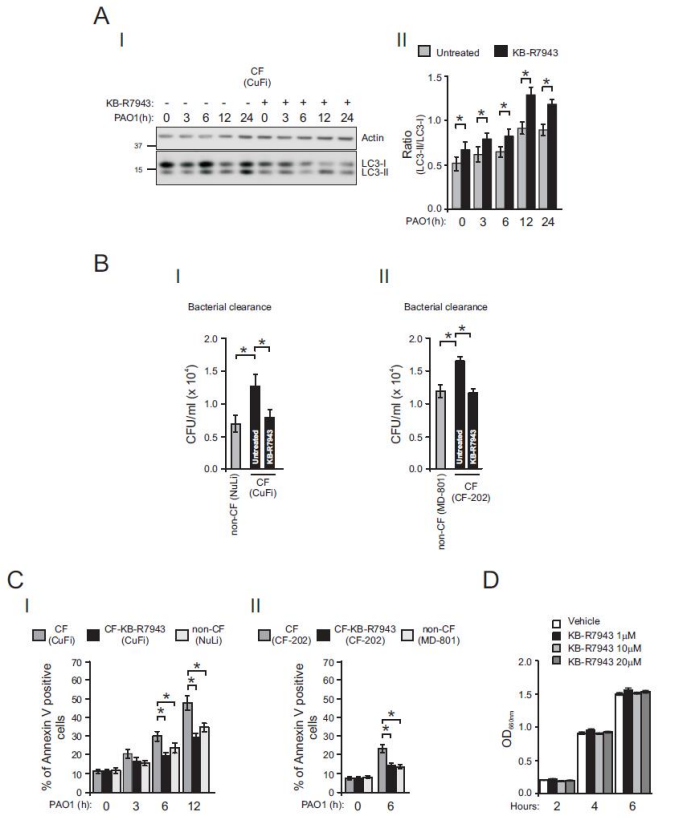

Supplementary figure 8: ***KB-R7943 confers cell resistance to pathogen infection restoring xenophagy in CF bronchial cells during P. aeruginosa infection.***

A) Effects of KB-R7943 on the autophagy in CuFi cells during pathogen infection. (I) The samples were probed on immunoblots for LC3 and actin as a loading control. (II) Bar chart shows the ratio LC3-II/LC3-I following quantification of signals from immunoblots (n=3). **B**) Effects of KB-R7943 on the xenophagy in CuFi cells (I) and in polarized primary patient-derived CF-202 cells (II). CF cells were pretreated with KB-R7943 one hour before infection with PAO1 at 100 MOI for 6 hours, then lysed after the addition of impermeable antibiotics and streaked on LB agar plates for the determination of intracellular CFUs (n=6 of independent experiments). (**C**) Effect of KB-R7943 on CF bronchial cell apoptosis, during *P. aeruginosa* infection, using annexin-V Alexa Fluor® 488/PI staining. Cell viability and death were evaluated using the Tali™ apoptosis kit and the Tali™ Image-based Cytometer. Bars show the percentage of CuFi and CF-202 (CF) and NuLi and MD-81 (non-CF) cells, respectively, that were annexin V–FITC positive (n=4 independent experiments). **D**) Bacteria were growth, in trypticase soy agar added with KB-R7943 at different concentration, at 37°C with shaking at 200 rpm and the OD660 values were monitored each two hours. The reported data are mean±SE of at least three independent experiments. *t*-Test used for indicated comparisons (* $p<0.05$).

Fig.S9

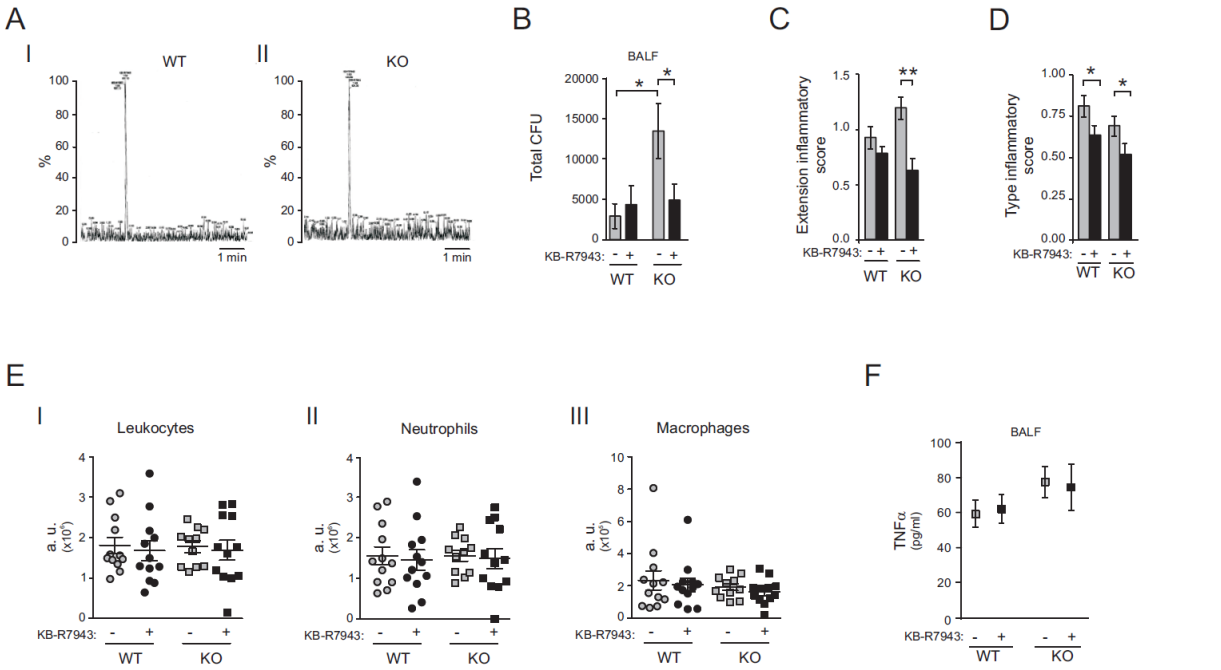

Supplementary figure 9: ***KB-R7943 mitigates the P. aeruginosa-triggered inflammatory response in CF mice without affecting the total number of inflammatory cells.***

A) Representative mass spectrum of KB-R7943 detected in plasma of WT (I) and CFTR-KO mice (II). **B**) Bacterial burden in BALF of KB-R7943-treated and untreated mice after two days from *P. aeruginosa* challenge is shown. The bars represent mean±SE of lung CFU in mice. Data were analyzed by two-way ANOVA and Tukey's post hoc test (* $p<0.05$, n=15-20 mice analyzed of three independent experiments). **C**) Graphs summarize histological scoring of inflammatory extension (n=60 of independent experiments) and **D**) Inflammatory type grading based on H&E staining (n=45 of independent experiments). Data were analyzed by *t*-Test used for indicated comparisons and by two-way ANOVA and Tukey's post hoc test (* $p<0.05$ and ** $p<0.01$). **E**) The number of total leukocytes and in particular of neutrophils and macrophages in the airways were analyzed in BALF from WT and CFTR-KO mice after two days of lung infection and pretreated with KB-R7943 (300 μg/kg). The horizontal and vertical lines represent mean±SE values (n=12 of independent experiments). **F**) Levels of TNFα in BALF from WT and CFTR-KO mice exposed to *P. aeruginosa* infection, treated with KB-R7943 (300 μg/kg) and vehicle, expressed as mean ±SE (n=14 of independent experiments).

Supplementary Material and Methods:

Mouse model of chronic infection and treatment

For the infection procedure, *P. aeruginosa* AA43 strain isolated from a CF patient before death, was embedded in agar-beads as previously described (1). Mice were anesthetized by an intraperitoneal injection of a solution of Avertin (2,2,2-tribromethanol, 97%) in 0.9% NaCl and administered at a volume of 0.015 ml/g body weight. Mice were placed in supine position. The trachea was directly visualized by ventral midline, exposed and intubated with a sterile, flexible 22-g cannula attached to a 1 ml syringe. An inoculum of 50µl of agar bead suspension, embedding $1.5x10^6$ CFU of AA43 strain, was implanted via the cannula into the lung. After inoculation, all incisions were closed by suture. Mice were treated with KB-R7943 (300µg/kg) or vehicle via aerosol administration by Penn-Century MicroSprayer® Aerosolizer every 12 hours starting one hour before infection. Two days post-infection (one hour post last treatment), mice were sacrificed. BALF was extracted with a 22-gauge venous catheter by washing the lungs with RPMI-1640 (Euroclone) with protease inhibitors (Complete tablets, Roche Diagnostic and PMSF, Sigma). An aliquot of BALF was serially diluted and plated on trypticase soy agar (TSA, Becton Dickinson). Total cells present in the BALF were counted, and a differential cell count was performed on cytospins stained with Diff Quick (Dade, Biomap, Italy). BALF was then centrifuged and supernatant tested for cytokines levels. Lungs were excised aseptically and homogenized in 2 ml PBS with protease inhibitor using the homogenizer gentleMACS^{TM} Octo Dissociator and dilutions spotted onto TSA plates and CFU determined after overnight growth at 37°C.

Mice were monitored twice per day for the piloerection, attitude, locomotion, breathing, curiosity, nasal secretion, grooming and dehydration. Mice that lost >20% body weight and had evidence of severe clinical disease, such as scruffy coat, inactivity, loss of appetite, poor locomotion, or painful posture, were sacrificed before the termination of the experiments with an overdose of carbon dioxide.

Lung histological analysis

In another group of mice, lungs were excised aseptically, fixed in formalin, and embedded in paraffin. Consecutive sections from the middle of the five lung lobes were stained by hematoxylin and eosin, examined using an Axioplan fluorescence microscope (Zeiss), and images were taken with a KS 300 imaging system (Kontron). Sections were blindly examined and scored by a pathologist. Histological score analysis of murine lungs was performed to: *i*) evaluate in a general manner the percentage of lung's parenchyma involvement in the inflammatory/infiltration process; *ii*) evaluate the distribution of inflammatory infiltrate between the aerate spaces and/or interstitial areas; *iii*) grade the amount of innate immune cells infiltration and BALT activation. Regarding the first two evaluations *i*), and *ii*) lung's sections were observed and scored at a magnification of ×100. For *iii*) evaluations, the assessment of cellular infiltrates and aggregation was obtained by scoring the number of immune cells (mononuclear cells, such as macrophages, lymphocytes, plasma cells, and neutrophils) at a magnification of ×400. The number of inflammatory cells was evaluated by using a visual analogue scale modified for murine pulmonary specimens, as described previously (2), and results are reported as the average for the entire specimen. When considerable heterogeneity of infiltration was evident in the same specimen, the mean for several areas was determined and the specimen was scored accordingly. Neutrophils and macrophages were classified as absent (score of 0) when there were no or fewer than 19 cells per high-power field (HPF) (at a magnification of ×400), mild (score of 1) for 20 to 49 cells per HPF, moderate (score of 2) for 50 to

99 cells per HPF, marked or severe (score of 3) for 100 to 200 cells or more per HPFs. Histological criteria for normal pulmonary characteristics included detection of no or only a few mononuclear cells per HPF and no or only a few scattered neutrophils in bronchioli and alveoli without tissue changes (no interstitial thickening or aggregates of lymphocytic infiltrates, and airways free from exudate). The number of inflammatory cells and of lymphoid aggregates, assessed at ×400 and ×100 magnification respectively, was scored and customized as previously described (3).

Histologic lesions of the respiratory bronchial epithelium were evaluated and scored for the presence or absence of ciliated columnar cells, goblet cells, edema, hyperplasia or metaplasia of epithelial cells, and lymphocytes infiltration (see also the scoring system to evaluate adaptive immunity), based on the previously described scoring system (4): presence of ciliated columnar epithelium, normal goblet cells, and no lymphocyte infiltration in respiratory epithelium (score 1); presence of focal lesions, some degenerative or necrotic epithelial cells, small focal areas lacking cilia, no lymphocyte infiltration in respiratory epithelium (score 2); multifocal areas lacking cilia accompanied by edema, degenerative and hyperplastic changes in epithelial cells, locally disrupted epithelial layer, infiltration of lymphocytes (score 3); diffuse or severe lesions showing replacement of normal ciliated columnar epithelial lining by the squamous to cuboidal epithelium without cilia, disrupted epithelial layer in many places, depletion of goblet cells, and infiltration of lymphocytes into respiratory epithelium (score 4). The sums of scores of bronchial lesions for mouse in one group were summed, and was used for statistical comparison of the severity lesions between the groups. Finally, concerning histological scores indicating an adaptive immune response, the presence of lymphoid nodules consisting of 5 to 7 lymphocyte-like cells (germinal centers) within areas of secondary bronchi and blood vessels, the intensity of dispersed lymphocyte infiltration in the interalveolar septa and interparabronchial septum and around the secondary bronchi as well as around the blood vessels was evaluated and recorded. The score was calculated as follow: no lymphocyte accumulation in interalveolar and interparabronchial septa, and very few germinal centers around secondary bronchi and blood vessels (score 0); accumulation of a few dispersed lymphocytes without the increase of the number of germinal centers (score1); moderate accumulation of lymphocytes in interalveolar and interparabronchial septa, increased size of germinal centers (group of 10–13 cells) around blood vessels (score 2); thickened interatrial septa in a large area of the lung, interparabronchial septa infiltrated with histiocytes and lymphocytes, and increased number of germinal centers (score 3). The sum of scores of the mice in one group was used for statistical comparison of the severity of bronchial lesions and mononuclear cells system activation between the groups. For BALT activation, the score was assessed at ×100, by calculating the total areas of BALT follicles evaluated inside each lung section, and subdividing the mean as follow: mean area of BALT follicle extension none (score 0); up to 0.008 square mm (score 1); up to 0.042 square mm (score 2); up to 0.4 square mm (score 3). For evaluation the degree of interstitial thickening and edema in lungs, sections were assessed evaluating the degree of interstitial eosinophilia, amorphous and hyaline aspect, with intersperse and not well-organized collagen fibers network. Elements of the pleura were excluded from the computations.

Graphical abstract

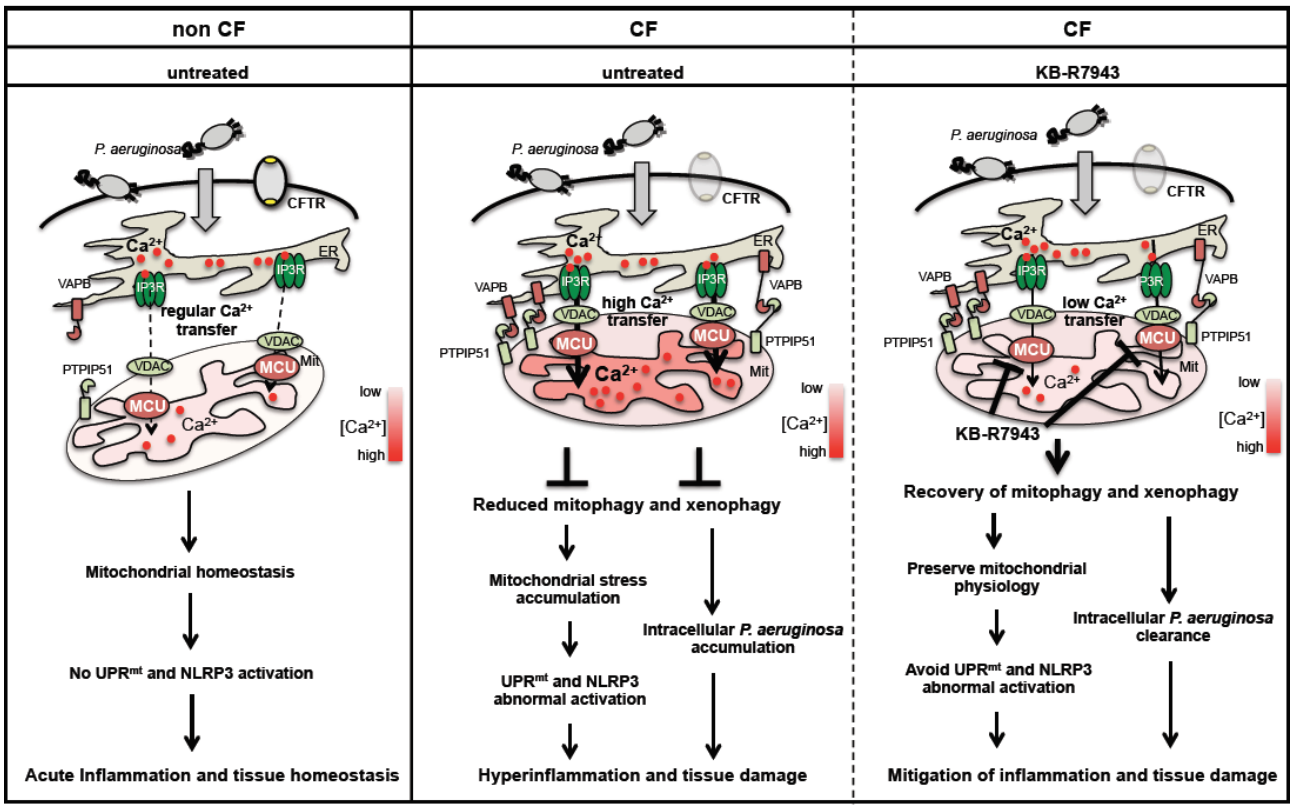

REFERENCES AND NOTES

1. J. S. Elborn, Cystic fibrosis. *Lancet* **388**, 2519–2531 (2016).

2. L.-C. Tsui, R. Dorfman, The cystic fibrosis gene: A molecular genetic perspective. *Cold Spring Harb. Perspect. Med.* **3**, a009472 (2013).

3. E. A. Roesch, D. P. Nichols, J. F. Chmiel, Inflammation in cystic fibrosis: An update. *Pediatr. Pulmonol.* , (2018).

4. R. Rubino, V. Bezzerri, M. Favia, M. Facchini, M. Tebon, A. K. Singh, B. Riederer, U. Seidler, A. Iannucci, A. Bragonzi, G. Cabrini, S. J. Reshkin, A. Tamanini, *Pseudomonas aeruginosa* reduces the expression of CFTR via post-translational modification of NHERF1. *Pflugers Arch.* **466**, 2269–2278 (2014).

5. L. R. Hoffman, B. W. Ramsey, Cystic fibrosis therapeutics: The road ahead. *Chest* **143**, 207–213 (2013).

6. M. E. Martino, J. C. Olsen, N. B. Fulcher, M. C. Wolfgang, W. K. O'Neal, C. M. P. Ribeiro, Airway epithelial inflammation-induced endoplasmic reticulum Ca^{2+} store expansion is mediated by X-box binding protein-1. *J. Biol. Chem.* **284**, 14904–14913 (2009).

7. A. Rimessi, V. Bezzerri, S. Patergnani, S. Marchi, G. Cabrini, P. Pinton, Mitochondrial Ca^{2+}−dependent NLRP3 activation exacerbates the *Pseudomonas aeruginosa*-driven inflammatory response in cystic fibrosis. *Nat. Commun.* **6**, 6201 (2015).

8. M. W. Pellegrino, A. M. Nargund, N. V. Kirienko, R. Gillis, C. J. Fiorese, C. M. Haynes, Mitochondrial UPR-regulated innate immunity provides resistance to pathogen infection. *Nature* **516**, 414–417 (2014).

9. J. E. Irazoqui, E. R. Troemel, R. L. Feinbaum, L. G. Luhachack, B. O. Cezairliyan, F. M. Ausubel, Distinct pathogenesis and host responses during infection of *C. elegans by P. aeruginosa and S. aureus*. *PLOS Pathog.* **6**, e1000982 (2010).

10. A. Tosco, F. De Gregorio, S. Esposito, D. De Stefano, I. Sana, E. Ferrari, A. Sepe, L. Salvadori, P. Buonpensiero, A. Di Pasqua, R. Grassia, C. A. Leone, S. Guido, G. De Rosa, S. Lusa, G. Bona, G. Stoll, M. C. Maiuri, A. Mehta, G. Kroemer, L. Maiuri, V. Raia, A novel treatment of cystic fibrosis acting on-target: Cysteamine plus epigallocatechin gallate for the autophagy-dependent rescue of class II-mutated CFTR. *Cell Death Differ.* **23**, 1380–1393 (2016).

11. C. Cárdenas, R. A. Miller, I. Smith, T. Bui, J. Molgó, M. Müller, H. Vais, K.-H. Cheung, J. Yang, I. Parker, C. B. Thompson, M. J. Birnbaum, K. R. Hallows, J. K. Foskett, Essential regulation of cell bioenergetics by constitutive $InsP_3$ receptor Ca^{2+} transfer to mitochondria. *Cell* **142**, 270–283 (2010).

12. J.-P. Decuypere, G. Bultynck, J. B. Parys, A dual role for Ca^{2+} in autophagy regulation. *Cell Calcium* **50**, 242–250 (2011).

13. A. Rimessi, M. Bonora, S. Marchi, S. Patergnani, C. M. T. Marobbio, F. M. Lasorsa, P. Pinton, Perturbed mitochondrial Ca^{2+} signals as causes or consequences of mitophagy induction. *Autophagy* **9**, 1677–1686 (2013).

14. R. D. Junkins, A. Shen, K. Rosen, C. McCormick, T.-J. Lin, Autophagy enhances bacterial clearance during *P. aeruginosa* lung infection. *PlOS ONE* **8**, e72263 (2013).

15. A. Luciani, V. R. Villella, S. Esposito, N. Brunetti-Pierri, D. Medina, C. Settembre, M. Gavina, L. Pulze, I. Giardino, M. Pettoello-Mantovani, M. D'Apolito, S. Guido, E. Masliah, B. Spencer, S. Quaratino, V. Raia, A. Ballabio, L. Maiuri, Defective CFTR induces aggresome formation and lung inflammation in cystic fibrosis through ROS-mediated autophagy inhibition. *Nat. Cell Biol.* **12**, 863–875 (2010).

16. V. Bezzerri, P. d'Adamo, A. Rimessi, C. Lanzara, S. Crovella, E. Nicolis, A. Tamanini, E. Athanasakis, M. Tebon, G. Bisoffi, M. L. Drumm, M. R. Knowles, P. Pinton, P. Gasparini, G. Berton, G. Cabrini, Phospholipase C-β3 is a key modulator of IL-8 expression in cystic fibrosis bronchial epithelial cells. *J. Immunol.* **186**, 4946–4958 (2011).

17. P. Prandini, F. De Logu, C. Fusi, L. Provezza, R. Nassini, G. Montagner, S. Materazzi, S. Munari, E. Gilioli, V. Bezzerri, A. Finotti, I. Lampronti, A. Tamanini, M. C. Dechecchi, G. Lippi, C. M. Ribeiro, A. Rimessi, P. Pinton, R. Gambari, P. Geppetti, G. Cabrini, Transient receptor potential ankyrin 1 channels modulate inflammatory response in respiratory cells from patients with cystic fibrosis. *Am. J. Respir. Cell Mol. Biol.* **55**, 645–656 (2016).

18. C. M. P. Ribeiro, The role of intracellular calcium signals in inflammatory responses of polarised cystic fibrosis human airway epithelia. *Drugs R D* **7**, 17–31 (2006).

19. A. Rimessi, V. Bezzerri, F. Salvatori, A. Tamanini, F. Nigro, M. C. Dechecchi, A. Santangelo, P. Prandini, S. Munari, L. Provezza, N. Garreau de Loubresse, J. Muller, C. M. P. Ribeiro, G. Lippi, R. Gambari, P. Pinton, G. Cabrini, PLCB3 loss of function reduces *Pseudomonas aeruginosa*-dependent IL-8 release in cystic fibrosis. *Am. J. Respir. Cell Mol. Biol.* **59**, 428–436 (2018).

20. C. Giorgi, S. Marchi, P. Pinton, The machineries, regulation and cellular functions of mitochondrial calcium. *Nat. Rev. Mol. Cell Biol.* **19**, 713–730 (2018).

21. C. Giorgi, A. Danese, S. Missiroli, S. Patergnani, P. Pinton, Calcium dynamics as a machine for decoding signals. *Trends Cell Biol.* **28**, 258–273 (2018).

22. A. Rimessi, C. Giorgi, P. Pinton, R. Rizzuto, The versatility of mitochondrial calcium signals: From stimulation of cell metabolism to induction of cell death. *Biochim. Biophys. Acta* **1777**, 808–816 (2008).

23. S. Marchi, S. Patergnani, S. Missiroli, G. Morciano, A. Rimessi, M. R. Wieckowski, C. Giorgi, P. Pinton, Mitochondrial and endoplasmic reticulum calcium homeostasis and cell death. *Cell Calcium* **69**, 62–72 (2018).

24. C. Giorgi, S. Missiroli, S. Patergnani, J. Duszynski, M. R. Wieckowski, P. Pinton, Mitochondria-associated membranes: Composition, molecular mechanisms, and physiopathological implications. *Antioxid. Redox Signal.* **22**, 995–1019 (2015).

25. R. Stoica, K. J. De Vos, S. Paillusson, S. Mueller, R. M. Sancho, K.-F. Lau, G. Vizcay-Barrena, W.-L. Lin, Y.-F. Xu, J. Lewis, D. W. Dickson, L. Petrucelli, J. C. Mitchell, C. E. Shaw, C. C. J. Miller, ER-mitochondria associations are regulated by the VAPB-PTPIP51 interaction and are disrupted by ALS/FTD-associated TDP-43. *Nat. Commun.* **5**, 3996 (2014).

26. P. Gomez-Suaga, S. Paillusson, R. Stoica, W. Noble, D. P. Hanger, C. C. J. Miller, The ER-Mitochondria Tethering Complex VAPB-PTPIP51 Regulates Autophagy. *Curr. Biol.* **27**, 371–385 (2017).

27. M. Lazarou, D. A. Sliter, L. A. Kane, S. A. Sarraf, C. Wang, J. L. Burman, D. P. Sideris, A. I. Fogel, R. J. Youle, The ubiquitin kinase PINK1 recruits autophagy receptors to induce mitophagy. *Nature* **524**, 309–314 (2015).

28. R. Garcia-Medina, W. M. Dunne, P. K. Singh, S. L. Brody, *Pseudomonas aeruginosa* acquires biofilm-like properties within airway epithelial cells. *Infect. Immun.* **73**, 8298–8305 (2005).

29. C. J. Fiorese, A. M. Schulz, Y.-F. Lin, N. Rosin, M. W. Pellegrino, C. M. Haynes, The Transcription Factor ATF5 Mediates a Mammalian Mitochondrial UPR. *Curr. Biol.* **26**, 2037–2043 (2016).

30. Z. Sheng, L. Ma, J. E. Sun, L. J. Zhu, M. R. Green, BCR-ABL suppresses autophagy through ATF5-mediated regulation of *mTOR* transcription. *Blood* **118**, 2840–2848 (2011).

31. J. Santo-Domingo, L. Vay, E. Hernández-SanMiguel, C. D. Lobatón, A. Moreno, M. Montero, J. Alvarez, The plasma membrane Na^+/Ca^{2+} exchange inhibitor KB-R7943 is also a potent inhibitor of the mitochondrial Ca^{2+} uniporter. *Br. J. Pharmacol.* **151**, 647–654 (2007).

32. A. Zsembery, J. A. Fortenberry, L. Liang, Z. Bebok, T. A. Tucker, A. T. Boyce, G. M. Braunstein, E. Welty, P. D. Bell, E. J. Sorscher, J. P. Clancy, E. M. Schwiebert, Extracellular zinc and ATP restore chloride secretion across cystic fibrosis airway epithelia by triggering calcium entry. *J. Biol. Chem.* **279**, 10720–10729 (2004).

33. T. Brustovetsky, M. K. Brittain, P. L. Sheets, T. R. Cummins, V. Pinelis, N. Brustovetsky, KB-R7943, an inhibitor of the reverse Na^+/Ca^{2+} exchanger, blocks N-methyl-D-aspartate receptor and inhibits mitochondrial complex I. *Br. J. Pharmacol.* **162**, 255–270 (2011).

34. T. P. Storozhevykh, Y. E. Senilova, T. Brustovetsky, V. G. Pinelis, N. Brustovetsky, Neuroprotective effect of KB-R7943 against glutamate excitotoxicity is related to mild mitochondrial depolarization. *Neurochem. Res.* **35**, 323–335 (2010).

35. B. M. Wiczer, R. Marcu, B. J. Hawkins, KB-R7943, a plasma membrane Na^+/Ca^{2+} exchanger inhibitor, blocks opening of the mitochondrial permeability transition pore. *Biochem. Biophys. Res. Commun.* **444**, 44–49 (2014).

36. K. B. Hisert, S. L. Heltshe, C. Pope, P. Jorth, X. Wu, R. M. Edwards, M. Radey, F. J. Accurso, D. J. Wolter, G. Cooke, R. J. Adam, S. Carter, B. Grogan, J. L. Launspach, S. C. Donnelly, C. G. Gallagher, J. E. Bruce, D. A. Stoltz, M. J. Welsh, L. R. Hoffman, E. F. McKone, P. K. Singh, Restoring cystic fibrosis transmembrane conductance regulator function reduces airway bacteria and inflammation in people with cystic fibrosis and chronic lung infections. *Am. J. Respir. Crit. Care Med.* **195**, 1617–1628 (2017).

37. M. A. Puertollano, E. Puertollano, G. A. de Cienfuegos, M. A. de Pablo, Dietary antioxidants: Immunity and host defense. *Curr. Top. Med. Chem.* **11**, 1752–1766 (2011).

38. R. Zhou, A. S. Yazdi, P. Menu, J. Tschopp, A role for mitochondria in NLRP3 inflammasome activation. *Nature* **469**, 221–225 (2011).

39. N. V. Kirienko, F. M. Ausubel, G. Ruvkun, Mitophagy confers resistance to siderophore-mediated killing by *Pseudomonas aeruginosa*. *Proc. Natl. Acad. Sci. U.S.A.* **112**, 1821–1826 (2015).

40. M. A. Qureshi, C. M. Haynes, M. W. Pellegrino, The mitochondrial unfolded protein response: Signaling from the powerhouse. *J. Biol. Chem.* **292**, 13500–13506 (2017).

41. M. Bonora, S. Patergnani, A. Rimessi, E. De Marchi, J. M. Suski, A. Bononi, C. Giorgi, S. Marchi, S. Missiroli, F. Poletti, M. R. Wieckowski, P. Pinton, ATP synthesis and storage. *Purinergic Signal* **8**, 343–357 (2012).

42. S. Böckler, B. Westermann, Mitochondrial ER contacts are crucial for mitophagy in yeast. *Dev. Cell* **28**, 450–458 (2014).

43. K. Mallilankaraman, C. Cárdenas, P. J. Doonan, H. C. Chandramoorthy, K. M. Irrinki, T. Golenár, G. Csordás, P. Madireddi, J. Yang, M. Müller, R. Miller, J. E. Kolesar, J. Molgó, B. Kaufman, G. Hajnóczky, J. K. Foskett, M. Madesh, MCUR1 is an essential component of mitochondrial Ca^{2+} uptake that regulates cellular metabolism. *Nat. Cell Biol.* **14**, 1336–1343 (2012).

44. M. A. Rodgers, J. W. Bowman, Q. Liang, J. U. Jung, Regulation where autophagy intersects the inflammasome. *Antioxid. Redox Signal.* **20**, 495–506 (2014).

45. M. Takahama, S. Akira, T. Saitoh, Autophagy limits activation of the inflammasomes. *Immunol. Rev.* **281**, 62–73 (2018).

46. D. M. Arduino, J. Wettmarshausen, H. Vais, P. Navas-Navarro, Y. Cheng, A. Leimpek, Z. Ma, A. Delrio-Lorenzo, A. Giordano, C. Garcia-Perez, G. Médard, B. Kuster, J. García-Sancho, D. Mokranjac, J. K. Foskett, M. T. Alonso, F. Perocchi, Systematic Identification of MCU Modulators by Orthogonal Interspecies Chemical Screening. *Mol. Cell* **67**, 711–723.e7 (2017).

47. T. Iwamoto, T. Watano, M. Shigekawa, A novel isothiourea derivative selectively inhibits the reverse mode of Na^+/Ca^{2+} exchange in cells expressing NCX1. *J. Biol. Chem.* **271**, 22391–22397 (1996).

48. H. Hagihara, Y. Yoshikawa, Y. Ohga, C. Takenaka, K.-Y. Murata, S. Taniguchi, M. Takaki, Na^+/Ca^{2+} exchange inhibition protects the rat heart from ischemia-reperfusion injury by blocking energy-wasting processes. *Am. J. Physiol. Heart Circ. Physiol.* **288**, H1699–H1707 (2005).

49. M. Matsunaga, M. Saotome, H. Satoh, H. Katoh, H. Terada, H. Hayashi, Different actions of cardioprotective agents on mitochondrial Ca^{2+} regulation in a Ca^{2+} paradox-induced Ca^{2+} overload. *Circ. J.* **69**, 1132–1140 (2005).

50. T. Iwamoto, S. Kita, A. Uehara, Y. Inoue, Y. Taniguchi, I. Imanaga, M. Shigekawa, Structural domains influencing sensitivity to isothiourea derivative inhibitor KB-R7943 in cardiac Nna^{+}/Ca^{2+} exchanger. *Mol. Pharmacol.* **59**, 524–531 (2001).

51. A. Scorziello, C. Savoia, M. J. Sisalli, A. Adornetto, A. Secondo, F. Boscia, A. Esposito, E. V. Polishchuk, R. S. Polishchuk, P. Molinaro, A. Carlucci, L. Lignitto, G. Di Renzo, A. Feliciello, L. Annunziato, NCX3 regulates mitochondrial Ca^{2+} handling through the AKAP121-anchored signaling complex and prevents hypoxia-induced neuronal death. *J. Cell Sci.* **126**, 5566–5577 (2013).

52. M. S. Amran, N. Homma, K. Hashimoto, Pharmacology of KB-R7943: A Na^{+}-Ca^{2+} exchange inhibitor. *Cardiovasc. Drug Rev.* **21**, 255–276 (2003).

53. F. Schweda, H. Seebauer, B. K. Krämer, A. Kurtz, Functional role of sodium-calcium exchange in the regulation of renal vascular resistance. *Am. J. Physiol. Renal Physiol.* **280**, F155–F161 (2001).

54. Z. Long, B. Chen, Q. Liu, J. Zhao, Z. Yang, X. Dong, L. Xia, S. Huang, X. Hu, B. Song, L. Li, The reverse-mode NCX1 activity inhibitor KB-R7943 promotes prostate cancer cell death by activating the JNK pathway and blocking autophagic flux. *Oncotarget* **7**, 42059–42070 (2016).

55. C. A. Hobbs, C. Da Tan, R. Tarran, Does epithelial sodium channel hyperactivity contribute to cystic fibrosis lung disease? *J. Physiol.* **591**, 4377–4387 (2013).

56. B. Liu, S. E. Peel, J. Fox, I. P. Hall, Reverse mode Na^{+}/Ca^{2+} exchange mediated by STIM1 contributes to Ca^{2+} influx in airway smooth muscle following agonist stimulation. *Respir. Res.* **11**, 168 (2010).

57. A. Criollo, M. C. Maiuri, E. Tasdemir, I. Vitale, A. A. Fiebig, D. Andrews, J. Molgó, J. Díaz, S. Lavandero, F. Harper, G. Pierron, D. di Stefano, R. Rizzuto, G. Szabadkai, G. Kroemer, Regulation of autophagy by the inositol trisphosphate receptor. *Cell Death Differ.* **14**, 1029–1039 (2007).

58. P. B. Gordon, I. Holen, M. Fosse, J. S. Røtnes, P. O. Seglen, Dependence of hepatocytic autophagy on intracellularly sequestered calcium. *J. Biol. Chem.* **268**, 26107–26112 (1993).

59. A. Rimessi, M. Previati, F. Nigro, M. R. Wieckowski, P. Pinton, Mitochondrial reactive oxygen species and inflammation: Molecular mechanisms, diseases and promising therapies. *Int. J. Biochem. Cell Biol.* **81**, 281–293 (2016).

60. C. Loriol, S. Dulong, M. Avella, N. Gabillat, K. Boulukos, F. Borgese, J. Ehrenfeld, Characterization of SLC26A9, facilitation of Cl^- transport by bicarbonate. *Cell. Physiol. Biochem.* **22**, 15–30 (2008).

61. M. Facchini, I. De Fino, C. Riva, A. Bragonzi, Long term chronic *Pseudomonas aeruginosa* airway infection in mice. *J. Vis. Exp.*, e51019 (2014).

62. A. Cersini, M. C. Martino, I. Martini, G. Rossi, M. L. Bernardini, Analysis of virulence and inflammatory potential of *Shigella flexneri* purine biosynthesis mutants. *Infect. Immun.* **71**, 7002–7013 (2003).

63. M. C. Martino, G. Rossi, I. Martini, I. Tattoli, D. Chiavolini, A. Phalipon, P. J. Sansonetti, M. L. Bernardini, Mucosal lymphoid infiltrate dominates colonic pathological changes in murine experimental shigellosis. *J. Infect. Dis.* **192**, 136–148 (2005).

64. M. J. Dykstra, S. Levisohn, O. J. Fletcher, S. H. Kleven, Evaluation of cytopathologic changes induced in chicken tracheal epithelium by Mycoplasma gallisepticum in vivo and in vitro. *Am. J. Vet. Res.* **46**, 116–122 (1985).